Mon. Not. R. Astron. Soc. **000**, 1–17 (2004) Printed 7 January 2014 (MN LaTeX style file v2.2)

The Lithium Depletion Boundary in NGC 2547 as a test of pre-main-sequence evolutionary models⋆

R.D. Jeffries and J.M. Oliveira
Astrophysics Group, School of Chemistry and Physics, Keele University, Keele, Staffordshire ST5 5BG, United Kingdom

Submitted August 20 2004

ABSTRACT
Intermediate resolution spectroscopy from the ESO Very Large Telescope is analysed for 63 photometrically selected low-mass (0.08-0.30 $M_{\odot}$) candidates of the open cluster NGC 2547. We have confirmed membership for most of these stars using radial velocities, and found that lithium remains undepleted for cluster stars with $I > 17.54 \pm 0.14$ and $K_s > 14.86 \pm 0.12$. From these results, several pre-main-sequence evolutionary models give almost model independent ages of 34-36 Myr, with a precision of 10 per cent. These ages are only slightly larger than the ages of 25-35 ($\pm$5) Myr obtained using the same models to fit isochrones to higher mass stars descending towards the zero age main sequence (ZAMS), both in empirically calibrated and theoretical colour-magnitude diagrams. This agreement between age determinations in different mass ranges is an excellent test of the current generation of low-mass pre-main sequence stellar models and lends confidence to ages determined with either method between 30 and 120 Myr.

Key words: stars: abundances – stars: late-type – open clusters and associations: individual: NGC 2547

1 INTRODUCTION

Absolute ages in young open clusters and star forming regions are difficult to determine and usually very model dependent, yet are crucial to solving many stellar evolution problems – from the lifetimes of protoplanetary disks and progression of angular momentum loss, to calibrating cooling models and the initial-final mass relation for white dwarfs. Nuclear turn-off ages from high mass stars may be uncertain by factors of two, depending on the treatment of core convection, rotation and mass loss (Chiosi, Bertelli & Bressan 1992; Meynet et al. 1993; Meynet & Maeder 1997, 2000). Ages from fitting isochrones to cool, low-mass stars, descending towards the ZAMS may be equally inaccurate: they depend on detailed modelling of stellar atmospheres, including molecular opacities, convection and turbulence (see Baraffe et al. 1998, 2002) and observational comparisons suffer from uncertainties in the conversion from model parameters ($L_{\rm bol}$ and $T_{\rm eff}$) to magnitudes and colours (e.g. Stauffer, Hartmann & Barrado y Navascués 1995).

The *Lithium Depletion Boundary* (LDB) is a new, important, and possibly less model dependent method for determining the ages of young clusters. The initial Li content of a low-mass star begins to burn in p, α reactions, as stars contract along PMS tracks and core temperatures reach 2.5×10^6 K. Below $0.065 M_{\odot}$, Li is never burned because the core does not become hot enough. At higher masses, the time taken to reach Li-burning temperatures is a sensitive function of mass and hence a *very sensitive function of luminosity* (Bildsten et al. 1997; Ushomirsky et al. 1998). Low-mass stars approaching the ZAMS are fully convective, so their entire Li content is then rapidly exhausted (in less than a few Myr after Li burning is initiated) and thus in a cluster, the luminosity at which photospheric Li remains undepleted can give a very precise age estimate and is most sensitive for ages of 10-200 Myr.

The small experimental uncertainties in the LDB method are due to the conversion from optical and near infrared magnitudes to luminosities via cluster distances and empirical bolometric corrections, and the difficulty in locating the LDB among a population of very faint, low-mass stars (see Jeffries & Naylor 2001). Systematic errors are likely to be quite small. Remarkably, different evolutionary models and even analytic calculations yield almost identical (to $\pm$10%) ages, despite very different treatments of atmospheres, convection, opacities and equations of state (see for example Burke, Pinsonneault & Sills 2004). It is this model

⋆ Based on observations collected with the VLT/UT2 Kueyen telescope (Paranal Observatory, ESO, Chile) using the FLAMES/GIRAFFE spectrograph (Observing run 072.D-0406A).

independence which makes it vital to measure the LDB in as many young clusters as possible. Such clusters would define empirical isochrones that could be used to link together and calibrate the uncertain physics in both high- and low-mass stellar evolution models.

LDB ages have so far only been determined for the Pleiades (125 ± 8 Myr), Alpha Per (90 ± 10 Myr) and IC 2391 (53 ± 5 Myr) clusters (Stauffer, Schultz & Kirkpatrick 1998; Stauffer et al. 1999; Barrado y Navascués, Stauffer & Patten 1999; Barrado y Navascués, Stauffer & Jayawardhana 2004). These ages are older by factors of $\simeq 1.5$ than nuclear turn-off ages determined from high mass evolutionary models with zero convective overshoot. The fractional discrepancy may become smaller towards younger ages (and hence higher masses at the turn-off), hinting that additional convective overshoot is mass-dependent.

For IC 2391, the LDB age is also about 15 Myr older than the age indicated by fitting isochrones to the low-mass ($0.3 < M < 1.2 M_{\odot}$) PMS cluster members. This may also be true for the cluster NGC 2547, which has a nuclear turn-off age of 55 ± 25 Myr (Jeffries & Tolley 1998), a low-mass isochronal age of 20-35 Myr (Naylor et al. 2002) a distance modulus of 8.10 ± 0.10 (Naylor et al. 2002) and a reddening, $E(B-V) = 0.06 \pm 0.02$ (Clariá 1982). A previous attempt to detect the LDB in NGC 2547 was made by Oliveira et al. (2003), but resulted in lower limits to the cluster age. No Li-rich objects were found for $I < 17.2$ and by considering the average spectrum of several cluster candidates there was some evidence that the LDB lay between $17.8 < I < 18.3$. This suggested that the LDB age of the cluster was certainly more than 30 Myr and probably more like 38-46 Myr and hence older than the low-mass isochronal age. Oliveira et al. suggested that this discrepancy might indicate shortcomings in the commonly used low-mass evolutionary models.

In this paper we present optical spectroscopy from the ESO Very Large Telescope (VLT) that unambiguously identifies a substantial population (~ 50) of very low-mass stars in NGC 2547 and now precisely determines the location of the LDB. In section 2 we discuss the selection of targets, the fibre spectroscopy performed at the VLT and the data reduction process. In section 3 we report measurements of relative radial velocities and the Li I 6708Å feature in the cluster candidates, and our assessment of cluster membership. Section 4 deals with the location of the LDB and the age of NGC 2547. The results are discussed in section 5 and conclusions drawn in section 6.

2 VLT FIBRE SPECTROSCOPY

2.1 Target selection

The targets for VLT fibre spectroscopy were chosen from the *RIZ* survey of Jeffries et al. (2004). This catalogue contains precise astrometric and photometric information for stellar objects in 0.855 square degrees around NGC 2547 and is substantially complete to $I = 19.5$. Fifty four targets were chosen from the lists of candidate cluster members with $16.4 < I < 19.1$ which were in turn selected from their photometric colours and proximity to empirically calibrated 30 Myr isochrones generated from the models of D'Antona & Mazzitelli (1997) and Baraffe et al. (2002) (see Jeffries et al. 2004 for details). Using an intrinsic distance modulus of 8.1 and extinction, $A_I = 0.112$ (Rieke & Lebofsky 1985), cluster members in this magnitude range will have approximate masses of 0.08-0.30 $M_{\odot}$ according to the models of Baraffe et al. (2002).

These targets are only a small, representative subset of a larger population of NGC 2547 cluster members in this magnitude range, that is spread over more than a square degree. A further nine objects were observed that were slightly more distant from the cluster isochrones and not classed as members by Jeffries et al., but which were also contained within the 25 arcminute diameter VLT field of view. The precision of the photometry is about ± 0.04 in I and ± 0.07 in $R-I$ for the faintest object in the sample (with $I = 19.05$), but is more like $\pm(0.01 - 0.02)$ in colour and magnitude for the majority.

2.2 Observations

The targets were observed on 19 and 20 January 2004 using the FLAMES instrument mounted on the VLT-Kueyen (UT2) 8.2-m telescope. The GIRAFFE spectrograph and MEDUSA fibre system were used in combination with the 600 lines mm^{-1} grating and an order sorting filter to give spectra with a resolving power of about 8000 over the wavelength range 6438Å $< \lambda <$ 7184Å. The MEDUSA system has 130 fibres, each with a projected diameter of 1.2 arcseconds on the sky, that can be positioned within a circular area of diameter 25 arcminutes.

The targets were observed in 8 separate observing blocks (OBs), each of which yielded 2589 s of observing time on sky and all of which were centred at RA = 08h 10m 06.6s, Dec = −49d 15m 43s. A number of fibre configurations were used, such that most objects (and all with $I > 18.5$) were observed in all 8 OBs, a few targets were observed in 5 or 6 OBs and one target (number 35 - see Table 1) was observed in only 2 OBs. This was done to maximise the number of targets observed at the required level of precision. Six of the OBs were obtained on 19 January 2004 between 03:14 UT and 08:43 UT. The other two OBs were obtained on 20 January 2004 between 03:09 UT and 07:28 UT. About 50 fibres which could not be allocated to useful targets were placed on blank sky regions in each configuration. The seeing measured at the telescope was 0.5-0.9 arcseconds and the moon was below the horizon during the observations. Flat-field, bias and Thorium-Argon arc lamp calibrations were performed at the start of each observing night.

2.3 Data Reduction

The calibrations and observational data were reduced using version 1.10 of the GIRAFFE pipeline software (Blecha et al. 2003). Master bias and flat-field calibrations were produced for each night along with fits tables containing the locations of the fibre spectra (from the master flat-field) on the 2K×4K EEV CCD detector and wavelength calibration solutions for all the fibres taken from the arc lamp spectra. Each target exposure was bias-subtracted, and scattered light was removed by modelling the remaining signal between the individual spectra. Target and blank sky spectra were extracted using an optimal algorithm. Pixel-to-pixel

and fibre-to-fibre sensitivity variations were corrected for by dividing by a normalised set of spectra extracted from the master flat-field using the same apertures. Note that no attempt is made to flux calibrate the spectra in an absolute sense, but that most of the instrumental response is removed by dividing by the flat-field continuum. The corrected spectra were then rebinned to a wavelength scale of 0.2Å per pixel, slightly larger than the average wavelength coverage of a single detector pixel.

Sky subtraction was achieved by taking the median of groups of five blank sky spectra and averaging these medians to form a master sky spectrum which could be subtracted from each target spectrum. The standard deviation among the continuum levels in the individual sky spectra was about 7 per cent (1-sigma). Part of this arises from uncertainties in the fibre-to-fibre sensitivity corrections, resulting largely from non-uniform illumination of the fibres by the flat-field lamp (L. Pasquini, ESO, private communication). There may also be a contribution from scattered continuum radiation from a bright, *spatially varying*, H II region which coincides with the NGC 2547 line of sight and is clearly visible in R-band images. The H II region is even more evident in the bright night-sky emission lines, where variations of 20-30 per cent are found even between sky fibres situated only a few arcminutes apart.

Uncertainties in the subtracted sky continuum are of no concern for this paper as far as measuring the continuum level close to the Li I 6708Å feature. The sky continuum is just equal to the signal from the targets at $I \simeq 19$ and hence for an unresolved line of width $\simeq 0.8$Å there may be an additional equivalent width error of about 0.05Å, which is smaller than the statistical errors in the equivalent width measurements even for the faintest targets (see section 3.3). However, the strong sky lines are up to 200 times stronger than the sky continuum and so sky-subtraction in the immediate vicinity of these wavelengths (Hα, S II 6717Å, 6731Å etc.) was more problematic.

Multiple spectra for targets were combined using an iterative technique that rejected pixels deviating by more than 5-sigma from from the average of pixels at the same wavelength in all the normalised spectra of that target. Three separate combinations were produced: all of the spectra; all spectra from 19 January 2004; and all spectra from 20 January 2004. Where only two spectra of an object existed in the combination, these spectra were simply summed. The theoretical levels of signal-to-noise ratio (SNR) achieved in the averaged spectra from all the target exposures, based on measurements of the CCD gain and readout noise and propagating errors in the bias subtraction, flat-fielding, scattered light subtraction and sky subtraction, ranged from 6 to more than 50 per 0.2Å pixel in the faintest and brightest targets respectively. A sample of our spectra covering the full range of wavelengths, colours and magnitudes is shown in Fig. 1.

3 ANALYSIS

3.1 Spectral Indices

To check that all the observed targets had spectral types appropriate for their colours, we calculated the TiO (7140Å) and CaH (6975Å) narrow band spectral indices (see Oliveira et al. 2003). These indices are temperature sensitive and we expect a smooth relationship between their values and the $R-I$ colour index of NGC 2547 cluster members.

None of our targets are found to deviate significantly from the trend defined by the bulk of the data. However, this is not unexpected. Any contamination in our sample is certain to be dominated by foreground field M-dwarfs with almost identical narrow band indices at the same colour (Jeffries et al. 2004). The CaH index does have some sensitivity to gravity but this is unlikely to distinguish between cool pre-main-sequence objects at 30-50 Myr and main-sequence dwarfs. Indeed, targets which are deemed cluster non-members by virtue of their relative radial velocities (see section 3.2) are indistinguishable from cluster members on the basis of these narrow band indices. Table 1 lists spectral types for our targets, estimated by comparing their TiO (7140Å) narrow band indices with the those measured for stars with known spectral type (see Oliveira et al. 2003). We estimate these spectral types are good to ± half a subclass.

3.2 Radial velocities

Although we were unable to obtain observations of radial velocity standard stars during our observations, the *relative* radial velocities (RVs) of our targets proved a useful tool to discriminate cluster members from non-members and also identify short period (of order 10 days or less) binary systems in those targets which show other indications of membership (i.e. a detection of Li – see section 3.3). Members of the cluster (bar short period binaries) should have RVs with a dispersion of order 1 $\mathrm{km\,s^{-1}}$ (Jeffries, Totten & James 2000), so given that we expect the bulk of our targets to be cluster members, selection in a narrow range of relative RVs should exclude the vast majority of non-members.

Radial velocities were calculated by cross-correlating the region $6950 < \lambda < 7150$Å which includes prominent molecular band heads and only a few very weak nebular emission lines and telluric features. We chose one of the targets (number 30 – see Table 1) with a good SNR and an intermediate colour and spectral type to act as the RV template for all the other objects. All the spectra from each night were cross-correlated with the spectrum of object 30 obtained on 19 January 2004. Hence most objects have two relative RV measurements.

The average relative RV for the cluster members and the precision of the RV measurements were estimated by considering the subsample of targets that were Li-rich and hence almost certain cluster members (see section 3.5), but excluding three objects which had clearly discrepant or varying RVs from night to night. We found an average RV of $(-0.9 \pm 0.3)\,\mathrm{km\,s^{-1}}$ with a standard deviation of $1.7\,\mathrm{km\,s^{-1}}$ on 19 January 2004 and an average RV of $(+0.0 \pm 0.6)\,\mathrm{km\,s^{-1}}$with a standard deviation of $2.6\,\mathrm{km\,s^{-1}}$ on 20 January 2004. As the combined data from 19 January had a higher SNR, the smaller standard deviation is expected.

Cluster members were required to have RVs within $n\sigma$ of the average RV of the Li-rich objects on 19 January 2004 and a consistent RV measured on 20 January 2004. The value of n was adjusted depending on the empirical SNR (defined in the next section) of the spectrum in question. For

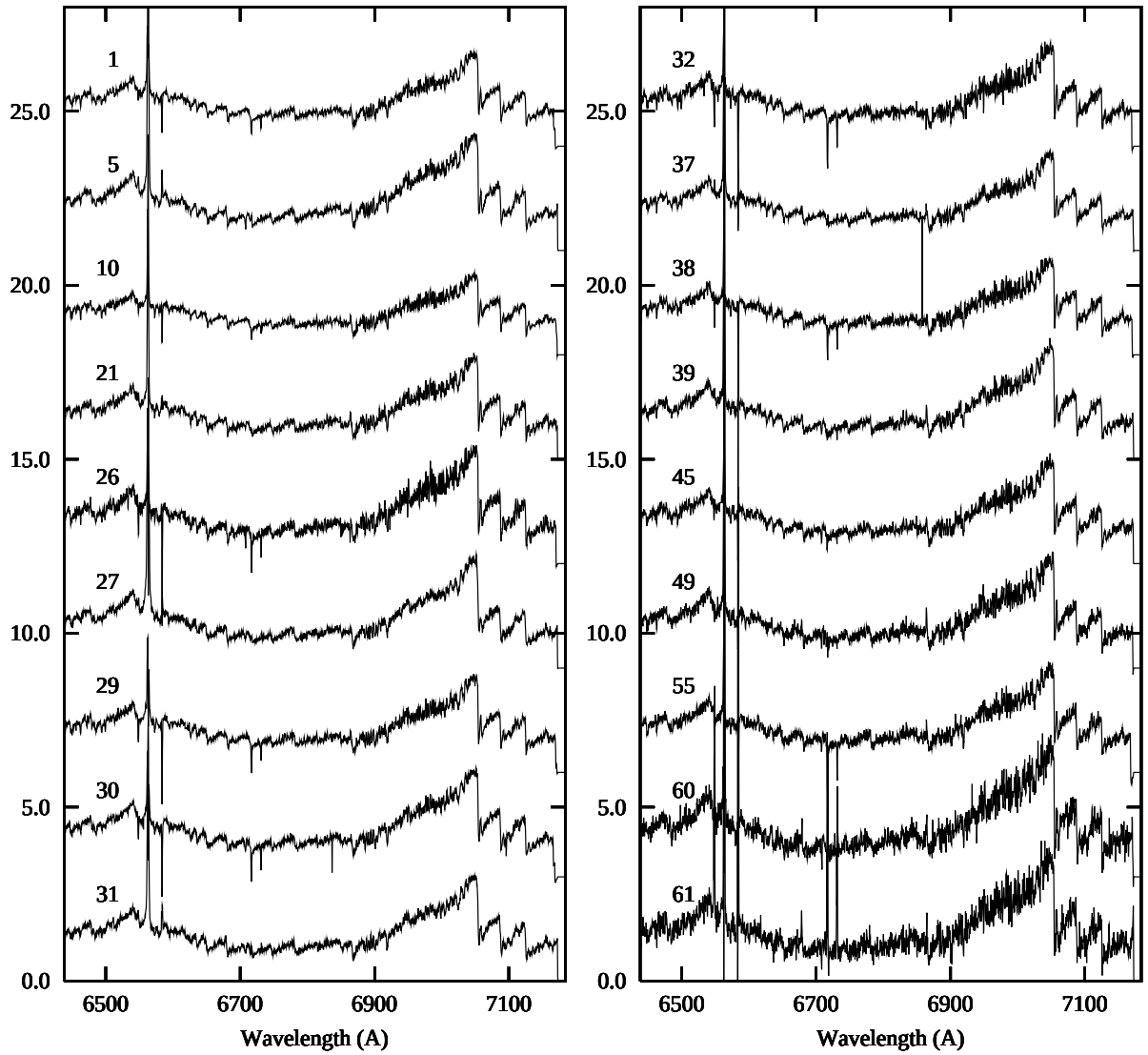

Figure 1. A representative sample of our reduced spectra covering the full range of colours and magnitudes. The spectra are normalised to unity at 6705Å and offset. The labels refer to the identifiers in Table 1.

SNR > 20, we used $n = 2$, for $10 <$ SNR < 20, $n = 3$ and for SNR < 10, $n = 4$. Before comparing the RVs from 19 and 20 January 2004, the mean discrepancy of $0.9\,\mathrm{km\,s^{-1}}$ was subtracted from the data taken on 20 January. The relative RVs for the targets on each night are listed in Table 1.

This process yielded 52 objects deemed to be cluster members, 9 objects deemed to be RV non-members and a further 2 objects where the RV appeared to be variable between data from the two nights. For some targets the cross-correlation function was markedly broadened, perhaps as a result of rapid rotation (see below) or binarity. These RV measurements are indicated in Table 1.

3.3 Lithium

The main aim of our experiment was to search for Li in the form of the Li I 6708Å resonance doublet. This feature should be strong in cool stars with undepleted Li – with an equivalent width (EW) of 0.5Å to 0.6Å according to the curves of growth presented by Zapatero-Osorio et al. (2002). Figure 2 shows a selection of our spectra in this wavelength region, where data combined from both nights are shown.

The EW of the 6708Å feature was estimated with respect to a pseudo-continuum defined by a linear fit to the data in the wavelength ranges 6700 to 6705Å and 6710 to 6713Å. The upper limit to this latter continuum region was chosen to coincide with a downturn in the spectra due to a molecular bandhead, but also to avoid regions within a few angstroms of the S II 6717Å sky line, which was poorly subtracted in many of our spectra and contained very noisy data in any case. The residuals to this linear fit gave an empirical estimate of the SNR which was used in turn to estimate either an uncertainty in the Li EW or a 2-sigma upper limit where no line was seen. The empirical SNR is bound to underestimate the true SNR of the spectra because there are molecular features in the pseudo-continuum that become stronger at cooler temperatures. Hence our EW uncertainty estimates and upper limits should be conservative

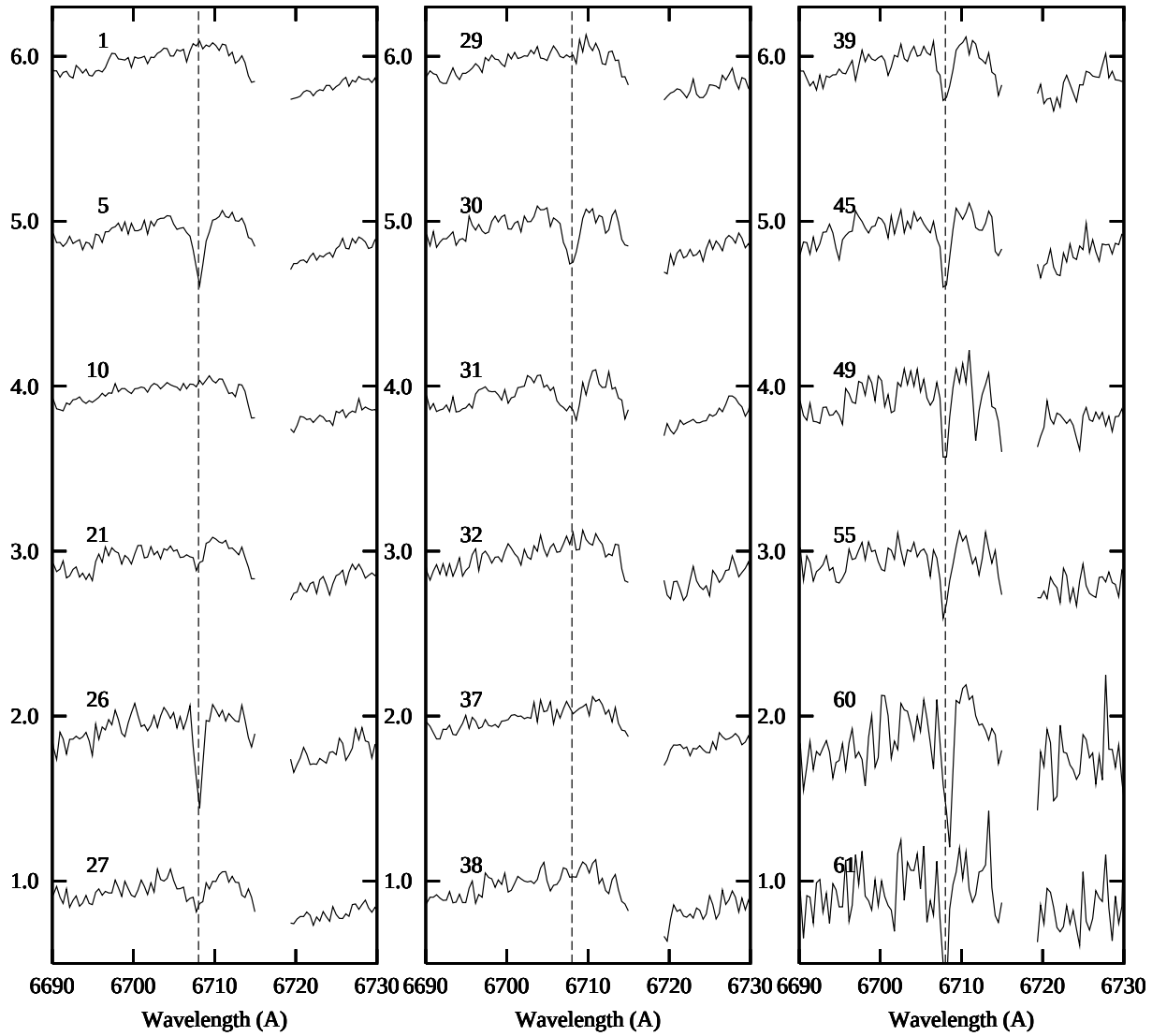

Figure 2. Representative spectra in the vicinity of the Li I 6708Å spectral feature. The spectra are labelled according to the identifiers in Table 1 and plotted in 0.4Å bins. The gaps in the spectra are the location of the prominent S II line found in the sky spectra, which could not be accurately subtracted. The spectra are normalised to unity around 6705Å and offset. The vertical dashed line indicates the expected position of the Li I 6708Å feature for members of NGC 2547.

and our EWs for the coolest stars may be systematically underestimated.

The EWs were estimated by fitting and integrating a Gaussian absorption feature beneath the linear continuum. Uncertainties were estimated according to the approximate formula

$$\Delta EW = \frac{\sqrt{\mathrm{FWHM} \times p}}{SNR}\,, \qquad (1)$$

where FWHM and p are the FWHM of the Gaussian and the size of the pixels in Å. The Li EWs or 2-sigma upper limits are listed in Table 1 along with the empirical SNR estimate. For target 63, which showed a large RV shift between the two nights, the quoted results are from the first night.

Most of our targets have FWHM in the range 0.7 to 1.0Å as expected from the resolving power of the spectrograph. A few objects showed Li lines which were much broader than this, with FWHM of 1.5-2.2Å. This is likely due to rapid rotation either in single objects simply because they are young (a phenomenon certainly seen in higher mass objects in the cluster – Jeffries et al. 2000) or because they are part of close, tidally locked binary systems. These broadened objects are indicated in Table 1. The data are of insufficient quality to estimate projected rotational velocities, but they must be of order $50\,\mathrm{km\,s^{-1}}$ to produce the broadening observed.

Table 1. Targets observed in this paper. The columns list identifiers used in this paper, identifiers from the catalogue of Jeffries et al. (2004) a "N" following the name indicates it was *not* considered a photometric member in that paper, positions, I magnitudes, $R-I$ and $I-Z$ colours from Jeffries et al. (2004), JHK_s magnitudes from 2MASS (Cutri et al. 2003), estimated spectral type (see section 3.1), relative radial velocity (nights 1 and 2, a "b" indicates a broadened cross-correlation function – see section 3.2), whether the radial velocity appears variable (V), the empirical SNR of the spectra around the Li 6708Å feature, the measured equivalent widths for this feature or a 2-sigma upper limit (a "b" indicates the line is broadened – see section 3.3) and our membership assessment status for the object – (1) radial velocity member with no Li, (2) radial velocity member with Li, (3) radial velocity non-member with Li, (4) radial velocity non-member with no Li. Photometric uncertainties are 0.01 to 0.04 mag in I and $I-Z$, 0.01 to 0.06 mag in $R-I$ and 0.04 to 0.20 mag in JHK_s (from brightest to faintest).

ID	J04 ID	RA (J2000)	DEC (J2000)	I	$R-I$	$I-Z$	J	H	K_s	SpT	RV_1 (km s^{-1})	RV_2 (km s^{-1})	Var?	SNR	Li EW (Å)	Status
1	17 629	8 09 17.721	−49 08 34.70	16.508	1.751	0.496	14.714	14.212	13.846	M4.5	−0.1	+0.1		30	< 0.03	1
2	9 467	8 11 05.423	−49 20 54.56	16.524	1.715	0.496	14.767	14.164	13.856	M4.5	−2.0	−3.2		34	< 0.03	1
3	13 605	8 10 50.499	−49 16 24.01	16.565	1.618	0.432	14.907	14.315	14.019	M4.5	+38.4	+38.1		41	< 0.02	4
4	13 586	8 09 29.032	−49 14 33.13	16.644	1.627	0.460	15.069	14.427	14.202	M4.0	−2.2	−1.0		50	< 0.02	1
5	8 515 N	8 10 11.757	−49 21 01.94	16.648	1.955	0.609	14.592	14.012	13.690	M5.5	+6.3	+6.5		27	0.61 ± 0.03 b	3
6	13 712	8 09 32.461	−49 11 13.09	16.697	1.687	0.499	14.894	14.421	14.057	M4.5	−1.3	−1.2		30	< 0.03	1
7	13 736	8 09 35.487	−49 13 03.54	16.742	1.739	0.518	15.008	14.445	14.071	M4.5	−2.8	−1.1		20	< 0.04	1
8	12 621	8 11 02.692	−49 11 08.69	16.753	1.693	0.446	15.084	14.422	14.076	M4.5	−2.0	−1.5		31	< 0.03	1
9	8 554	8 10 05.623	−49 26 25.49	16.763	1.664	0.461	15.010	14.360	14.133	M4.5	−2.8	−2.0		30	< 0.03	1
10	12 626	8 10 53.561	−49 11 43.20	16.816	1.607	0.448	15.217	14.703	14.238	M4.0	−1.0	−0.6		41	< 0.02	1
11	18 729	8 10 12.134	−49 04 31.80	16.864	1.698	0.465	15.234	14.549	14.205	M4.5	−1.0	−2.1		27	< 0.03	1
12	13 715	8 10 25.353	−49 11 18.68	16.918	1.834	0.558	14.982	14.433	14.131	M5.0	−1.7	−1.3		24	< 0.04	1
13	18 738	8 10 02.437	−49 05 13.40	16.935	1.648	0.449	15.269	14.658	14.351	M4.5	−1.9	−0.9		28	< 0.03	1
14	14 884	8 09 11.922	−49 14 43.11	16.946	1.745	0.481	15.177	14.629	14.422	M4.5	−0.8	−2.6		21	< 0.04	1
15	13 676	8 10 49.791	−49 08 20.02	16.988	1.701	0.491	15.245	14.714	14.414	M4.5	−1.8	−1.5		24	< 0.04	1
16	7 681	8 09 09.250	−49 20 42.77	16.999	1.644	0.469	15.358	14.761	14.404	M4.5	−2.7	−0.5		13	< 0.07	1
17	12 863 N	8 10 46.949	−49 15 21.64	17.038	1.607	0.486	15.290	14.645	14.349	M4.5	−2.5	−1.8		21	< 0.04	1
18	12 738	8 10 52.997	−49 07 16.53	17.061	1.802	0.548	15.208	14.605	14.174	M5.5	+0.9	+1.8		17	< 0.06	1
19	14 918	8 09 13.184	−49 17 38.79	17.077	1.711	0.499	15.326	14.737	14.506	M4.5	−1.8	+0.1		24	< 0.04	1
20	13 892	8 10 14.521	−49 10 23.64	17.125	1.732	0.515	15.299	14.681	14.504	M4.5	−0.3	−2.0		22	< 0.04	1
21	8 604	8 10 21.472	−49 17 48.61	17.149	1.799	0.536	15.300	14.670	14.458	M5.0	−2.1	−5.7		25	0.16 ± 0.03 b	1
22	13 931	8 09 51.086	−49 12 18.48	17.162	1.751	0.504	15.332	14.697	14.496	M4.5	−0.9	−2.7		19	< 0.05	1
23	8 679 N	8 10 17.675	−49 23 29.74	17.165	1.626	0.449	15.476	14.802	14.622	M4.0	+8.6	+7.9		18	< 0.05	4
24	7 727 N	8 09 24.619	−49 24 17.27	17.179	1.631	0.422	15.539	14.989	14.699	M4.0	+48.1	+46.7		28	< 0.03	4
25	13 922	8 10 04.600	−49 11 39.09	17.210	1.749	0.506	15.308	14.784	14.601	M4.5	−2.7	−1.7		22	< 0.04	1
26	12 752	8 10 58.886	−49 08 05.92	17.225	1.897	0.564	15.364	14.721	14.331	M5.5	+2.9			17	0.59 ± 0.03	2
27	8 655	8 10 46.890	−49 21 34.10	17.226	1.867	0.593	15.184	14.649	14.291	M5.5	−1.5	−0.3		19	0.36 ± 0.04 b	2
28	13 1148	8 09 56.050	−49 11 16.46	17.233	1.731	0.515	15.463	15.029	14.556	M4.5	−1.1	−2.3		18	< 0.05	1
29	12 810	8 11 07.003	−49 12 23.83	17.241	1.724	0.481	15.485	14.930	14.482	M4.5	−1.6	−1.0		20	< 0.04	1
30	13 906	8 10 03.099	−49 11 02.76	17.252	1.948	0.559	15.273	14.675	14.353	M5.0	+0.0	+1.3		19	0.47 ± 0.04 b	2
31	7 694	8 09 50.218	−49 21 15.89	17.291	1.819	0.556	15.486	14.782	14.540	M5.0	−0.1	−1.5		18	0.49 ± 0.04 b	2
32	12 774	8 11 11.865	−49 10 16.63	17.304	1.800	0.468	15.507	15.015	14.721	M5.0	−0.5	−0.9		19	< 0.06	1
33	9 760	8 10 36.428	−49 17 01.34	17.309	1.725	0.493				M4.5	+8.5	+8.8		22	< 0.04	4
34	14 1143	8 09 23.534	−49 16 27.44	17.318	1.674	0.541	15.537	14.923	14.675	M4.5	−1.7			11	< 0.08	1
35	12 792	8 11 11.678	−49 11 12.35	17.331	1.766	0.497	15.571	15.053	14.203	M4.5	−1.7			10	< 0.08	1
36	12 1127	8 11 05.846	−49 16 25.31	17.398	1.812	0.496	15.481	14.898	14.575	M5.0	−2.2	−4.5		17	< 0.06	1
37	14 1530	8 09 44.267	−49 18 43.97	17.398	1.734	0.511	15.509	15.126	14.879	M5.0	−0.3	−2.4		22	< 0.04	1
38	12 1000	8 11 03.987	−49 10 02.00	17.489	1.719	0.472	15.826	15.232	14.756	M4.5	−1.8	−0.9		18	< 0.06	1
39	8 770	8 10 12.072	−49 17 41.61	17.576	1.797	0.557	15.754	15.008	14.654	M5.0	−0.8	−0.9		16	0.44 ± 0.04 b	2
40	7 909 N	8 09 12.400	−49 22 28.02	17.653	1.684	0.440	15.973	15.356	15.087	M4.5	+11.2	+5.6		21	< 0.04	4
41	18 1436	8 10 16.488	−49 03 36.78	17.692	1.854	0.584	15.636	15.125	14.851	M6.0	−3.0	−0.2		10	0.41 ± 0.04	2
42	12 1202	8 10 46.139	−49 06 28.53	17.721	1.784	0.532	16.143	15.450	15.030	M4.5	−1.0	−1.5		5	0.76 ± 0.10	2
43	9 1011	8 11 09.442	−49 18 45.47	17.757	1.752	0.495	16.227	15.472	14.861	M4.5	+16.7 b	+16.3		14	< 0.06	4
44	14 1473	8 09 29.481	−49 16 40.12	17.803	1.763	0.535	15.947	15.308	14.991	M5.0	−3.9 b	0.0 b		19	0.44 ± 0.10 b	2
45	9 1039	8 10 57.646	−49 19 58.28	17.844	1.804	0.512 7	16.068	15.197	15.176	M5.0	−0.9	+0.4		14	0.50 ± 0.03	2
46	8 1183	8 10 17.868	−49 26 14.62	17.850	1.847	0.527	16.007	15.502	15.002	M5.0	−0.9	−0.4		10	0.40 ± 0.04	2
47	8 1274	8 09 43.775	−49 16 50.06	17.859	1.894	0.594	15.964	15.176	15.021	M6.0	−2.2	−3.1		13	0.38 ± 0.04	2
48	13 1165	8 10 41.234	−49 12 22.11	17.864	1.836	0.569	15.904	15.211	14.888	M5.5	−2.3	−2.2		10	0.24 ± 0.06	2
49	9 1595	8 10 53.286	−49 16 48.65	18.083	1.933	0.579	16.010	15.698	15.120	M5.0	−1.7	−4.0		9	0.51 ± 0.05	2
50	18 1480 N	8 09 53.162	−49 05 37.98	18.088	1.731	0.515	16.408	15.511	15.424	M5.0	+13.4	+4.4	V	11	< 0.08	4
51	17 1549 N	8 09 42.579	−49 04 39.69	18.149	1.749	0.505	16.419	15.916	15.722	M5.0	+10.0	+13.0		7	< 0.12	4
52	13 1850	8 09 50.801	−49 14 09.95	18.190	1.792	0.563				M5.0	−2.4	+0.4		8	0.52 ± 0.05	2
53	7 1474	8 09 08.079	−49 21 59.71	18.243	1.929	0.583	16.283	15.278	15.468	M6.0	−0.9	−2.1		9	0.47 ± 0.05	2
54	13 1790 N	8 09 46.870	−49 11 36.54	18.250	1.782	0.668	16.390	15.617	15.377	M5.0	+1.7	−0.9		9	0.52 ± 0.05	2
55	13 1776	8 10 08.240	−49 11 00.57	18.268	1.902	0.576	16.244	15.832	15.705	M5.0	−0.9	−0.6		10	0.40 ± 0.04	2
56	13 1828	8 10 01.843	−49 12 58.95	18.298	1.937	0.613	16.323	15.573	15.588	M5.5	−1.5			9	0.38 ± 0.06 b	2
57	7 1425	8 09 26.816	−49 20 08.19	18.383	1.958	0.643	16.365	15.772	15.498	M5.5	−2.8	−2.6		8	0.71 ± 0.06	2
58	7 1991	8 09 47.146	−49 26 33.24	18.564	2.088	0.674				M6.5	−1.5	+3.2		6	0.66 ± 0.07	2
59	12 2131	8 11 11.511	−49 11 08.98	18.565	2.043	0.569	16.520	15.832	14.586	M6.0	+2.6	−5.2		5	0.69 ± 0.09	2
60	14 2399 N	8 09 04.030	−49 18 43.54	18.633	1.976	0.716	16.281	15.889	15.526	M6.0	+8.0			7	0.94 ± 0.09 b	3
61	7 1914	8 09 46.706	−49 23 24.75	18.805	1.964	0.625	16.600	15.975	15.592	M6.0	−2.2	−1.4		5	0.72 ± 0.08	2
62	7 2365	8 09 34.569	−49 23 53.49	18.964	2.054	0.551				M6.0	+0.5	+7.5		3	0.60 ± 0.14	2
63	12 2833	8 11 21.619	−49 16 25.86	19.051	1.937	0.557				M6.0	+12.1	+83.0	V	3	< 0.28	4

3.4 Hα emission

Hα emission was seen in almost all our sky-subtracted spectra and in principle could be used as an additional membership criterion (e.g. Barrado y Navascués et al. 2004). However, whilst chromospheric Hα emission is expected from NGC 2547 members it would also be expected from a large fraction of any possible field M-dwarf contaminants with similar spectral types (Gizis, Reid & Hawley 2002). Unfortunately the presence and strength of Hα emission could not be accurately measured because the Hα emission line present in the sky spectrum is *much* stronger. The peak intensity of the Hα in the mean sky spectrum is 20-200 times the continuum intensity around Hα in our targets. Furthermore, the strength of the sky Hα emission varies by 20-30 per cent from fibre to fibre because of the background H II region (see section 2.3), resulting in effective EW errors of a few Angstroms even in the brightest stars of our sample. Slit spectroscopy will be required to obtain accurate estimates of chromospheric Hα emission in these stars.

What we were able to do was search for extended Hα emission beyond the wings of the sky line. In particular, White & Basri (2003) have shown that emission lines with a full width at 10 per cent of maximum of more than $270\,\mathrm{km\,s^{-1}}$ are indicative of ongoing accretion activity. Such objects would also typically have emission EWs of more than 20Å and hence extended emission wings easily visible in our spectra. Following the method detailed in Kenyon et al. (2004) we simulated a Gaussian Hα emission line with an EW of 20Å and full width at 10 per cent of maximum of $270\,\mathrm{km\,s^{-1}}$ for each of our spectra. No emission beyond this simulated profile (appropriately broadened for those objects thought to be rapid rotators – see section 3.3) was found. This result is not surprising. Jeffries et al. (2000) found no accretion signatures in higher mass objects in NGC 2547 and a recent *Spitzer* survey of the cluster by Young et al. (2004) finds less than 7 per cent of the low-mass cluster members have inner dust discs betrayed by an infrared excess. Nevertheless, combined with the precise LDB age derived for the cluster in this paper, NGC 2547 provides a useful upper limit to the lifetime of this early phase of stellar evolution.

3.5 Cluster membership

The measurements discussed above allow an assessment of cluster membership. First, we assume that the 23 objects showing an Li feature with an EW > 0.2Å and an RV consistent with cluster membership are cluster members. The rationale is that curves of growth presented by Zapatero-Osorio et al. (2002) suggest that the Li abundance is depleted by about a factor of 100 or less in these objects (see section 4), which is also the criterion we will adopt for judging the location of the LDB. Field M dwarfs are extremely unlikely to show an Li feature of this strength.

In addition there are two stars which show Li at this level but have an RV inconsistent with cluster membership. One of these (star 60) is probably a short period binary member of the cluster, the other (star 5) is unlikely to be a cluster member based on its colour and magnitude (see section 6.2). The 9 objects which show no Li and which have an RV inconsistent with cluster membership could be cluster binaries though this is unlikely. Five of these objects are fainter than our estimate of the LDB (see section 5) and should have exhibited Li if they were members and some of the others look unlikely to be cluster members on the basis of their colours and magnitudes (see section 6.2). Until there is further evidence we classify all these objects as non-members.

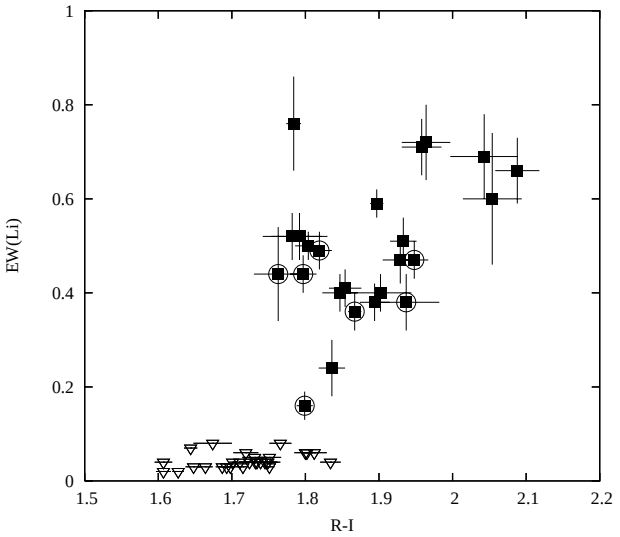

Figure 3. Li EWs versus $R-I$ colour for Li-rich and Li-poor RV members of NGC 2547. Downward pointing triangles indicate 2-sigma upper limits. Encircled points are those with significant rotational broadening – see section 3.3.

Finally, there are 29 objects with an RV consistent with cluster membership but showing no Li. These are very likely to be cluster members, although given the $\sim 10\,\mathrm{km\,s^{-1}}$ range over which cluster members are selected, it is possible that one or two contaminating non-members remain in this subset. There are unlikely to be more than this because we see no Li-poor, RV members *fainter* than the location of the LDB.

4 LITHIUM ABUNDANCES

We have estimated Li abundances, A(Li) (where A(Li) = log[N(Li)/N(H)]+12), for those objects which are RV members of the cluster. We use the curves of growth for cool stars presented by Zapatero-Osorio et al. (2002), and extended to A(Li)= 0.0 by Pavelenko & Zapatero-Osorio (private communication), in order to convert our EW values into Li abundances. The difficulties in doing this are described extensively in Jeffries et al. (2003), the main problem being that the definition of the pseudo-continuum used to derive the EW is not necessarily consistent between objects measured at different spectral resolutions or with different degrees of rotational broadening. It is also unknown to what extent there are model-dependent systematic errors in the cool atmospheres used to determine the curves of growth. For these reasons the *absolute* values of the Li abundances should be treated with caution.

To estimate $T_{\rm eff}$ values for our objects we have used an empirical relationship between intrinsic $R-I$ and $T_{\rm eff}$ defined by making a 120 Myr isochrone from the Chabrier

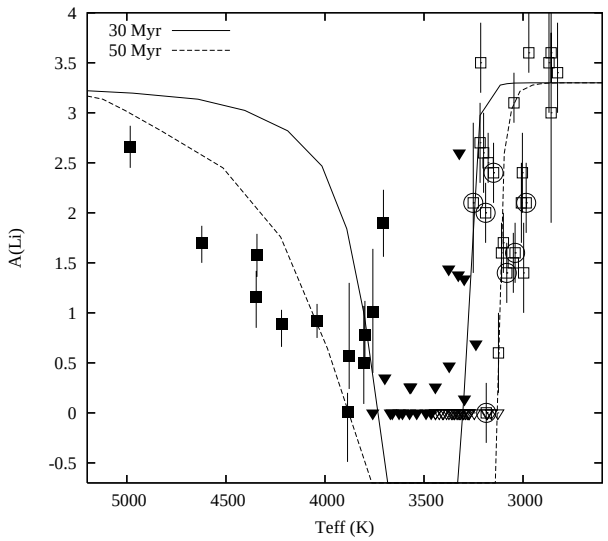

Figure 4. Li abundances versus $T_{\rm eff}$ for RV members of NGC 2547 from this paper (open symbols, encircled points indicate those with significant rotational broadening – see section 3.3) and from Jeffries et al. (2003 - filled symbols). Downward pointing triangles indicate 2-sigma upper limits. For comparison we show model predictions for the progression of Li depletion at 30 and 50 Myr, taken from the models of Chabrier & Baraffe (1997).

& Baraffe (1997) evolutionary models fit published Pleiades RI data at a distance of 132 pc (see section 6.3.2 for details). This relationship is shown in Fig. 10 and the $T_{\rm eff}$ values for the cluster members (derived assuming that $E(R-I) = 0.043$) are given in Table 2. Statistical uncertainties which arise from uncertainties in the $R-I$ photometry are small. However to allow for some variability we assign uncertainties of ± 100 K for the purpose of estimating possible Li abundance errors. The Li abundances were then obtained using a bicubic spline interpolation of the curves of growth. Many of our EW upper limits imply Li abundances that fall *well* below the lowest value in our grid, but we conservatively assign an upper limit of A(Li)< 0.0 to these. The statistical errors in the abundances were found by perturbing the EW and $T_{\rm eff}$ by their error bars and combining the two sources of error in quadrature. The EW uncertainty is dominant because the curves of growth become nearly independent of $T_{\rm eff}$ for $T_{\rm eff} < 3500$ K. For this reason, systematic uncertainties in the $T_{\rm eff}$ scale, which are quite likely to be of order 100-200 K at these cool temperatures, are not important. Li abundances and uncertainties are listed in Table 2.

In Figs 3 and 4 we show plots of the Li EWs versus $R-I$ colour and Li abundances versus $T_{\rm eff}$ for the NGC 2547 RV members. In the latter plot we have also included Li abundances for higher mass objects in the cluster derived using the same curves of growth (from Jeffries et al. 2003). A number of points arise from these two figures.

(1) There is a clear pattern of undetectable Li for warmer stars ($R-I < 1.75$). At slightly cooler temperatures there exist stars both with and without detectable Li and then for $R-I > 1.84$ only Li-rich objects are found.

(2) The overall pattern of Li depletion agrees qualitatively (but not quantitatively) with those predicted by PMS evolutionary models (see also Fig. 9 and the discussion in Jeffries et al. 2003). In particular the sharp upturn at cooler temperatures - the LDB - is present. However it is impossible to define a precise or accurate age for NGC 2547 on the basis of Fig. 4 because: (i) objects with and without Li co-exist at the crucial temperatures because of scatter caused by photometric errors, variability and unresolved binarity; (ii) the $T_{\rm eff}$ at the LDB *is* model dependent by of order ± 100 K (see Table 3), which translates to significant age uncertainties; (iii) there are systematic uncertainties of a similar size in the conversion from $R-I$ to $T_{\rm eff}$. These problems are solved in the next section by considering the data in the Hertzsprung-Russell diagram and finding the *luminosity* of the LDB.

(3) There appears to be a scatter in the Li abundances at low temperatures and even among the subset of objects with luminosities well below the LDB. This scatter arises directly from a spread in the EWs at a given colour. We believe that the spread in the EWs is real. Although some readers may question whether the approximation of equation 1 is strictly valid, it is unlikely to underestimate the EW errors by the factor of three that would be required to make them consistent with no spread. Systematic EW uncertainties are likely to be a monotonic function of $T_{\rm eff}$ and should not introduce scatter at a given colour. A similar Li EW scatter has been observed by Zapatero-Osorio et al. (2002) and Kenyon et al. (2004) for very low mass stars with $T_{\rm eff} < 3500$ K in the young σ Orionis cluster and by Barrado y Navascués et al. (2004) in IC 2391, but the spectra here are of higher quality and more importantly, taken at a homogeneous and relatively high resolution.

Whether the spread in abundances is real is a different matter. There is no theoretical explanation of such a scatter. All evolutionary models predict a sharp change from no Li to essentially cosmic Li over a small temperature range. There should be few, if any, transitional objects[1]. Instead we think this problem may be related to our understanding of the upper atmosphere of very cool stars. Because the Li feature is saturated in these cool dwarfs it is very susceptible to NLTE effects or perhaps overionization caused by an overlying chromosphere (e.g. Houdebine & Doyle 1995). This would cause a weakening of the Li feature in the most active stars and it is notable that: (i) the peak levels of Li abundance are roughly that expected for the cosmic Li abundance A(Li)$\simeq 3.3$; (ii) the rapid rotators tend to have lower Li EWs and abundances, although it would be difficult to discount problems with blending and continuum definition as an explanation for this. Given slit spectroscopy (to overcome the Hα sky subtraction problems) or very deep X-ray observations it should be possible to look for an inverse correlation between Li strength and chromospheric/coronal activity.

(4) Despite the scatter, the objects do still clearly bifurcate between those objects with Li (with an EW> 0.2Å) and those with much lower upper limits. This division corresponds roughly to where 99 per cent of the original Li has

[1] Target number 21 with a weak but detectable Li line and A(Li)$= 0.0 \pm 0.3$ may be an example of a transitional object, but could also be an example of an unresolved binary system with one component above and one component below the LDB.

Table 2. Effective temperatures derived from the intrinsic $R-I$ colour and Li abundances (where A(Li)= log[N(Li)/N(H)] + 12) obtained from the curves of growth of Zapatero-Osorio et al. (2002) for RV members of NGC 2547 (status 1 and 2 objects from Table 1). Columns 1 and 4 are the identifiers used in Table 1.

ID	$T_{\rm eff}$ (K)	A(Li)	ID	$T_{\rm eff}$ (K)	A(Li)
1	3272	< 0.0	31	3149	$2.4^{+0.3}_{-0.3}$
2	3328	< 0.0	32	3184	< 0.0
4	3423	< 0.0	34	3374	< 0.0
6	3361	< 0.0	35	3246	< 0.0
7	3291	< 0.0	36	3160	< 0.0
8	3354	< 0.0	37	3299	< 0.0
9	3386	< 0.0	38	3322	< 0.0
10	3442	< 0.0	39	3189	$2.0^{+0.3}_{-0.3}$
11	3348	< 0.0	41	3099	$1.7^{+0.3}_{-0.3}$
12	3127	< 0.0	42	3214	$3.5^{+0.4}_{-0.3}$
13	3402	< 0.0	44	3251	$2.1^{+0.8}_{-0.7}$
14	3282	< 0.0	45	3176	$2.5^{+0.3}_{-0.2}$
15	3345	< 0.0	46	3109	$1.6^{+0.3}_{-0.3}$
16	3406	< 0.0	47	3049	$1.5^{+0.3}_{-0.3}$
17	3442	< 0.0	48	3124	$0.6^{+0.4}_{-0.4}$
18	3180	< 0.0	49	3003	$2.4^{+0.4}_{-0.4}$
19	3333	< 0.0	52	3199	$2.6^{+0.4}_{-0.4}$
20	3303	< 0.0	53	3008	$2.1^{+0.4}_{-0.4}$
21	3186	$0.0^{+0.3}_{-0.3}$	54	3217	$2.7^{+0.4}_{-0.4}$
22	3272	< 0.0	55	3040	$1.6^{+0.3}_{-0.3}$
25	3275	< 0.0	56	2997	$1.4^{+0.5}_{-0.4}$
26	3046	$3.1^{+0.3}_{-0.2}$	57	2971	$3.6^{+0.4}_{-0.2}$
27	3082	$1.4^{+0.3}_{-0.3}$	58	2826	$3.4^{+0.5}_{-0.4}$
28	3304	< 0.0	59	2869	$3.5^{+0.5}_{-0.5}$
29	3314	< 0.0	61	2963	$3.6^{+0.4}_{-0.3}$
30	2984	$2.1^{+0.4}_{-0.3}$	62	2858	$3.0^{+0.8}_{-1.1}$

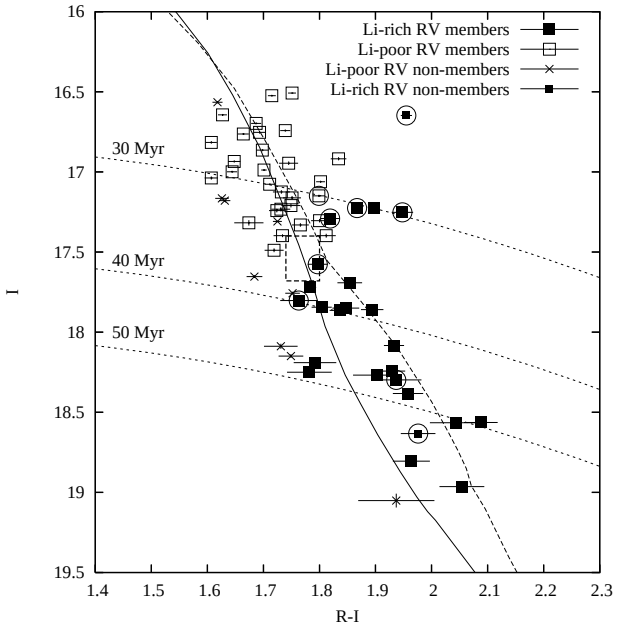

Figure 5. I,R-I colour-magnitude diagram for our targets. Open squares represent objects with an RV consistent with cluster membership but which have no Li, filled squares are those RV members with Li, small filled squares are Li-rich stars with an RV discrepant from the cluster and crosses represent objects with discrepant velocities and no Li. Encircled points represent those objects with discernible rotational broadening (see section 3.3). The solid line is an empirically calibrated (see text) 30 Myr isochrone generated from the models of Baraffe et al. (2002), the dashed line is a similar isochrone generated from the D'Antona & Mazzitelli (1997) models. We assume an intrinsic cluster distance modulus of 8.10 and a reddening $E(R-I) = 0.043$. The dashed box indicates our estimate of the position and uncertainty of the LDB. The dotted contours show isochrones (derived from the Chabrier & Baraffe 1997 models) corresponding to the location of the LDB in this diagram.

been depleted and we will use this to define the location of the LDB in the next section.

5 THE LITHIUM DEPLETION BOUNDARY AGE OF NGC 2547

5.1 The location of the LDB

Figures 5, 6 and 7 show the targets plotted in the I versus $R-I$, I versus $I-Z$ and K_s versus $I-K_s$ colour-magnitude diagrams (CMDs). Objects classified as Li-rich members, RV members with no Li, non-members on the basis of their RV or Li-rich objects with discrepant RVs are represented with different symbols. There is considerable scatter in these diagrams with no clear PMS locus visible – the isochronal ages discussed later in this paper are derived from stars of higher mass (see section 6.3.2). There are probably several sources of this scatter including binarity, rapid rotation, variability due to magnetic activity and photometric uncertainties.

There is however a clear pattern among the Li abundances. The brighter objects are Li-poor – all RV cluster members with $I < 17.22$ have no Li. The fainter objects are Li-rich – all RV cluster members with $I > 17.57$ have Li. However, there are both Li-poor and Li-rich objects between these two limits which potentially confuse the location of the LDB. Three of the four Li-rich objects in this region have broad Li lines suggesting rapid rotation which could result in them appearing brighter and redder than suggested by a PMS isochrone for slowly rotating stars (Pinsonneault et al. 1998). Alternatively their location in all three CMDs suggests that these are unresolved binary systems, which constitute roughly 30 per cent of the cluster population at these colours (Jeffries et al. 2004). Perhaps a clearer way of looking at the data is to note that while there may be several reasons why a star with Li lies above the single star locus in the CMD, there are none (beyond photometric error) that would cause a star without Li to lie below the single star locus. The faintest object without Li has $I = 17.49$ and two others have $I = 17.40$. This suggests that the LDB must be at $I \geqslant 17.4$. We contend that the LDB of NGC 2547 is at $I = 17.54 \pm 0.14$ and at colours of $R-I = 1.77 \pm 0.03$ and $I-Z = 0.53 \pm 0.02$. Similar considerations lead us to place the LDB at $K_s = 14.86 \pm 0.12$ and $I-K_s = 2.70 \pm 0.10$. These locations are represented by the boxes in Figs. 5, 6 and 7.

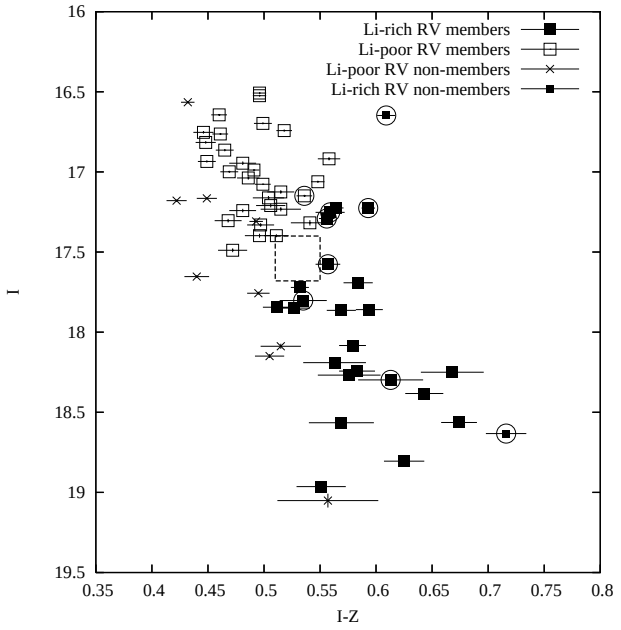

Figure 6. I,I-Z colour-magnitude diagram. Symbols are as in Fig. 5.

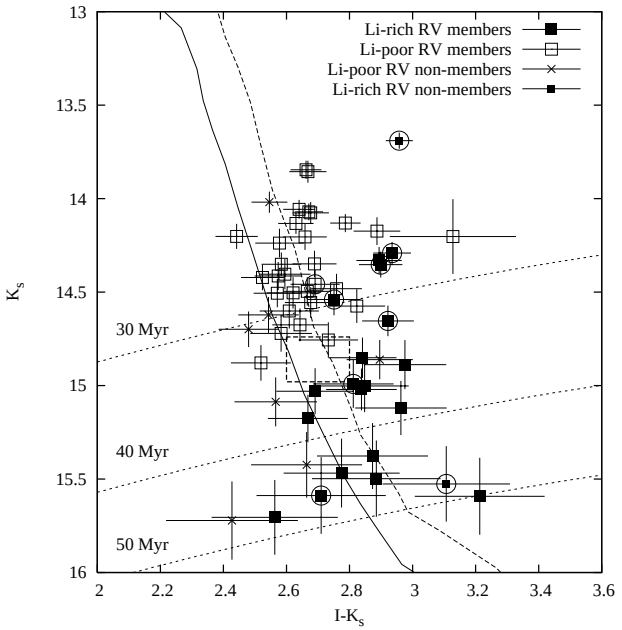

Figure 7. K_s,$I-K_s$ colour-magnitude diagram. Symbols are as in Fig. 5. The solid and dashed lines are 31.6 Myr and 20.0 Myr isochrones with colours and magnitudes taken directly from the models of Baraffe et al. (2002) and assuming an intrinsic distance modulus of 8.10 and $E(I-K_s) = 0.092$. The dotted contours show isochrones (derived from the Chabrier & Baraffe 1997 models) corresponding to the location of the LDB in this diagram.

5.2 Age estimates

The LDB location defined above can now be used to estimate the age of NGC 2547. The approach we take is the same as that described in Oliveira et al. (2003). Briefly, we use empirical relations between bolometric correction (for I or K_s) and colour ($R-I$ or $I-K_s$), along with the appropriate distance modulus, extinction and reddening (see section 1 and below) to calculate the absolute I or K_s magnitude of the LDB at any age, where we assume that the LDB represents the point at which 99 per cent of the initial Li has been depleted and hence the EW of the Li I feature has dropped below about 0.2Å. The age estimate can be performed for different evolutionary models. We note that our K_s magnitudes are on the 2MASS system and were converted to the CIT system (see Carpenter 2001) for the purposes of these calculations.

Uncertainties in the derived age are produced by several factors (see Jeffries & Naylor 2001). The ones we include in our analysis are: (1) The uncertainty in the position of the LDB in the CMD. These were estimated in the previous section and probably represent uncertainties of more than 1 sigma. (2) Systematic errors in the photometric calibration. These are important for I, $R-I$ and $I-K_s$. Jeffries et al. (2004) estimated external uncertainties for stars with $R-I > 1.5$ of up to ±0.10 mag in I and $R-I$ and hence there will be a systematic uncertainty of ±0.10 in the $I-K_s$ colours also. We assume a negligible external error for the K_s magnitudes. (3) We assume an uncertainty in the reddening $E(B-V) = 0.06 \pm 0.02$ (Clariá 1982) and hence that $E(R-I) = 0.043\pm0.014$, $E(I-K_s) = 0.092\pm0.031$ and extinctions of $A_I = 0.112 \pm 0.037$ and $A_K = 0.021 \pm 0.007$ (Rieke & Lebofsky 1985). (4) We assume an uncertainty in the intrinsic distance modulus of 8.10 ± 0.10 mag (see Jeffries & Tolley 1998; Naylor et al. 2002).

Table 3 list the results of these estimates for the solar metallicity evolutionary models of Chabrier & Baraffe (1997), D'Antona & Mazzitelli (1997), Siess, Dufour & Forestini (2000) and Burke et al. (2004). The uncertainties quoted include all the effects discussed above, which are added in quadrature[2]. Table 3 also gives the bolometric magnitude of the LDB, and the masses and $T_{\rm eff}$ at the LDB for each model.

As a comparison, we have also recalculated the LDB age of IC 2391 using our models and bolometric corrections. The LDB location was found by Barrado y Navascués et al. (2004) to be at $I = 16.22 \pm 0.10$, $R-I = 1.90 \pm 0.05$ and $K_s = 13.49\pm0.10$, $I-K_s = 2.75\pm0.10$. An intrinsic distance modulus of 5.95 ± 0.10 and reddening equal to that of NGC 2547 were also assumed. The LDB ages and parameters for IC 2391 are also given in Table 3.

In addition to the random error bars quoted on the ages in Table 3, there are other small systematic uncertainties affecting the LDB age scale as a whole – the gravity dependence of the bolometric correction and the exact level of Li depletion that the LDB corresponds to (see Burke et al. 2004). The theoretical models of Baraffe et al. (2002) yield I-band bolometric corrections as a function of colour and age (and hence gravity). It seems that the relationship between bolometric correction and $R-I$ is more age sensitive, with bolometric corrections lower by about 0.05 mag

[2] This assumes the sources of uncertainty are independent. This is unlikely to be true for the distance modulus and reddening which are correlated in the sense that a larger assumed reddening leads to a larger distance modulus via main sequence fitting and both lead to a smaller LDB age.

for stars at 30 Myr compared with 5 Gyr. The effect is limited to about 0.02 mag in the $I - K_s$ relation. Because the bolometric corrections we use are derived from high gravity field dwarfs a small adjustment to the bolometric corrections may be required. However, changes of this size would lead to LDB ages that were younger by only ~ 1 Myr. Similarly, Li depletion is so rapid that whether the LDB corresponds to 90 per cent depletion or 99.9 per cent depletion changes the LDB ages by only ± 1 Myr.

The ages in Table 3 show very close agreement both in terms of the ages using bolometric corrections deduced from the $R-I$ and $I-K_s$ colours and between ages derived from different models incorporating different physics. Taking the average result from both colours, the age of NGC 2547 ranges from 34 Myr to 36 Myr and the age of IC 2391 from 48 Myr to 53 Myr. The youngest ages in both cases are given by the D'Antona & Mazzitelli (1997) models. The difference in LDB age between IC 2391 and NGC 2547 is very consistent at 14-17 Myr.

As a final estimate of the LDB age we compared the absolute I and K_s magnitudes at the LDB directly with the models of Baraffe et al. (2002), remembering to convert the 2MASS magnitudes to the CIT system predicted by the models. In other words we are using *theoretical* bolometric corrections produced by the cool model atmospheres. The results for NGC 2547 and IC 2391 are listed in the last column of Table 3 and are very close to the estimates based on empirical bolometric corrections and the same evolutionary models (those of Chabrier & Baraffe 1997).

6 DISCUSSION

6.1 Comparison with Oliveira et al. (2003)

The analysis of Oliveira et al. (2003) arrived at a slightly older lower limit to the LDB age for NGC 2547 than we have found in this paper. Oliveira et al. found no evidence for a population of Li-rich objects with $I < 17.2$, although they did find a few examples of Li detections of brighter stars which might be either binary members of the cluster or perhaps not members of the cluster at all – see below. At fainter magnitudes there were a few tentative Li detections, but to place limits on the location of the LDB, Oliveira et al. averaged the spectra of targets with $17.3 < I < 17.8$ and with $I \geqslant 17.8$ separately. Evidence for an Li line was found in the average spectrum of the fainter sample, but not the brighter. Hence Oliveira et al. placed the LDB at $17.8 < I < 18.3$ and derived an age at least 3 Myr older than in this paper.

With the benefit of hindsight and in the light of the *much* better data obtained with VLT/GIRAFFE we can explain the probable cause of this discrepancy. We have found that the LDB is at $I = 17.54 \pm 0.14$, but 5 of the 10 objects in the $17.3 < I < 17.8$ sample of Oliveira et al. are brighter than this and hence unlikely to be Li rich. In addition we see from Fig. 5 that some level of contamination of the sample is also likely, such that perhaps 1-2 of the 5 objects with $17.54 < I < 17.8$ might be non-members and hence Li-poor. Given this, it is not hard to see why Li may not have been detected in the average spectrum of this subsample. On the other hand, the fainter sample should all be Li-rich , apart from contamination by Li-poor non-members at the level of $\leqslant 25$ per cent, and hence an Li detection would be expected.

There are also some discrepancies between the strengths of Li detected in this paper and those measured in Oliveira et al. (2003). We have observed three of the stars claimed to be Li-rich by Oliveira et al. Of these, we also detect Li in star 31 (= Oliveira no.75, O75) and star 42 (= O91). But, we find a very low upper limit to the Li EW of star 50 (= O100), where Oliveira et al. claim a significant detection. We have also observed six stars with a significant Li detection – stars 5(=O46), 27(=O73), 39(=O85), 41(=O89), 45(=92) and 53(=O106) for which Oliveira et al. found upper limits to the Li EW. Of these, two have a detection consistent with the previous upper limit (stars 27 and 53), but the other four have Li EWs greater than the previous 2-sigma upper limit. Three of these (stars 39, 41 and 45) were classed as non-members by Oliveira et al. on the basis that their narrow band spectroscopic indices (the same as those used in this paper) were too low for stars of their colour. It now seems clear that the "non-members" found by Oliveira et al. were almost certainly instances of under-subtracted sky, because even the contaminants in the photometrically selected cluster candidates have spectroscopic indices similar to those of cluster members. An under-subtracted sky will result in lower spectroscopic indices, dilution of any Li EW and an erroneously optimistic assessment of the SNR of the spectrum. Hence it is not surprising that stars classed as non-members in Oliveira et al. do not have Li detections.

6.2 Cluster membership and contamination

The work of Jeffries et al. (2004) in determining the mass function of NGC 2547 relied solely on photometric criteria to select cluster candidates. The spectroscopic results presented here offer an opportunity to check those photometric criteria and to estimate the amount of contamination present in a photometrically selected sample.

Figure 8 is an I versus $R-I$ CMD showing the catalogue of stars from which Jeffries et al. (2004) selected cluster candidates, their photometrically selected cluster candidates and symbols representing the status of stars that are analysed in this paper. Note that the cluster candidates were also selected on the basis of their positions in the I versus $I-Z$ and $R-I$ versus $I-Z$ diagrams (see Jeffries at al. for details). There are several points arising from Fig. 8.

(1) Looking at the distribution of RV selected members and RV non-members from this paper and comparing them with the distribution of photometrically selected candidates it appears that the photometric selection criteria employed by Jeffries et al. (2004) were quite appropriate. The presence of a "line" of five RV non-members *just below* the lower boundary of the cluster candidate distribution suggests that this boundary is well chosen, although we have also found two RV members (one Li-rich) near this boundary which were not photometrically selected as cluster candidates.

(2) The upper boundary of the photometric selection is less well explored by our spectroscopic data. However this has lesser implications for the completeness and contamination of the photometrically selected sample because the density of stars in the CMD decreases rapidly towards brighter magnitudes.

(3) Looking at spectroscopically observed stars which

Table 3. The LDB ages for NGC 2547 and IC 2391 using the I vs $R-I$ and K vs $I-K$ CMDs using different models and a summary of model parameters at the LDB.

		Chabrier & Baraffe (1997)	D'Antona & Mazzitelli (1997)	Siess et al. (2000) $z = 0.02$	Burke et al. (2004)	Baraffe et al. (2002) theoretical
NGC 2547						
LDB ages (Myr)	I vs $R-I$	35.4 ± 3.3	34.0 ± 3.7	36.2 ± 3.4	36.1 ± 4.4	36.3 ± 2.8
	K_s vs $I-K_s$	34.4 ± 2.7	33.8 ± 2.8	35.4 ± 2.6	35.4 ± 3.1	35.0 ± 2.6
Parameters at the LDB	M_{bol}[1]	9.58 ± 0.16	9.58 ± 0.16	9.58 ± 0.16	9.58 ± 0.16	9.63 ± 0.16
	Mass[1] ($M_\odot$)	0.17 ± 0.02	0.17 ± 0.02	0.15 ± 0.02	0.17 ± 0.01	0.17 ± 0.02
	$T_{\rm eff}$[1] (K)	3250 ± 30	3140 ± 20	3230 ± 40	3240 ± 40	3240 ± 30
IC 2391						
LDB ages (Myr)	I vs $R-I$	49.1 ± 4.9	47.3 ± 4.3	49.6 ± 4.8	52.5 ± 5.7	50.8 ± 3.9
	K_s vs $I-K_s$	50.4 ± 3.8	48.5 ± 3.2	50.5 ± 3.5	54.1 ± 4.4	49.6 ± 3.8
Parameters at the LDB	M_{bol}[1]	10.34 ± 0.14	10.34 ± 0.14	10.34 ± 0.14	10.34 ± 0.14	10.36 ± 0.14
	Mass[1] ($M_\odot$)	0.12 ± 0.01	0.12 ± 0.01	0.11 ± 0.01	0.12 ± 0.01	0.12 ± 0.01
	$T_{\rm eff}$[1] (K)	3140 ± 30	3070 ± 20	3100 ± 30	3150 ± 40	3130 ± 30

1 - these are averages from the very similar results for the two diagrams

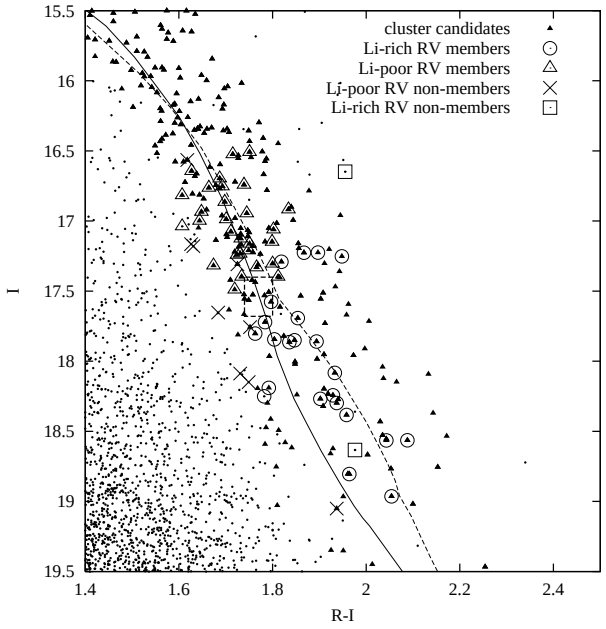

Figure 8. I,R-I colour-magnitude diagram for our targets superimposed on the general population towards NGC 2547, showing those objects identified as photometric cluster candidates by Jeffries et al. (2004). The solid line shows the empirically calibrated 30 Myr isochrones used to select members, which were generated from the models of Chabrier & Baraffe (1997 – solid line) and D'Antona & Mazzitelli (1997 – dashed line). Photometric selection also made use of the I vs $I-Z$ and $R-I$ vs $I-Z$ diagrams.

are also photometrically selected candidates we find four RV non-members (plus another RV non-member which is Li-rich and a probable cluster binary – star 60). In contrast we have found 50 RV members among the photometrically selected cluster candidates of which perhaps only 1-2 are random contaminants (none of which will be Li-rich). Hence the level of contamination among the photometrically selected cluster candidates is only about 10-15 per cent for the central regions of the cluster in the magnitude interval $16.5 < I < 19$. Given that we have observed nearly all the cluster candidates within the VLT/GIRAFFE field of view, this translates into a spatial density of about 30 ± 15 contaminants per square degree in this magnitude range, or 45 ± 18 if we assume there are an additional 2 contaminants among the Li-poor RV members. This compares reasonably well, though is a little lower than the estimates from Jeffries et al. (2004) of 80 per square degree based on a population synthesis or the 64 ± 26 per square degree based on the number of photometric cluster candidates found in regions offset from the cluster. Differences in contamination levels of this size would have no significant effect on the mass and luminosity functions for NGC 2547 determined by Jeffries et al. (2004).

(4) There is scope to improve the precision of the LDB location in the CMDs. There are a further 8 photometric cluster candidates that we have not observed that lie *inside* the LDB error box in the I versus $R-I$ CMD. However, the contributions to the error budget from uncertainties in the cluster distance and uncertain photometric calibrations for very cool stars play an equal role in the precision of the LDB age estimate.

(5) Star 5 is Li-rich but quite clearly not a photometric member of the cluster in any of the CMDs and not an RV member either. This star is too far above the cluster locus to be a a binary member. A single star of this colour would have to be younger than 50 Myr to have preserved its Li and such stars should be quite rare among the general field population. One possibility is that star 5 is a low-mass member of the Vela OB2 association which is sparsely spread over a ~ 10 degree diameter and which encompasses NGC 2547. Vela OB2 is at a distance of ~ 400 pc (de Zeeuw et al. 1999) and has an age of a few Myr. A population of low-mass, Li-rich PMS stars has been found in this association by Pozzo et al. (2000, 2001). If star 5 were at a distance

of 400 pc, then its position in the CMDs suggests an age of about 4 Myr (Baraffe et al. 2002), in excellent agreement with this hypothesis. Furthermore, star 5 has an RV which is 7.3 km s^{-1} larger than NGC 2547 average, which itself has a mean heliocentric RV of $+12.8 \pm 1.0$ km s^{-1} (Jeffries et al. 2000). Thus the heliocentric RV of star 5 is 20.1 ± 1.0 km s^{-1}, very close to the heliocentric RV of 18 km s^{-1} obtained for the Vela OB2 PMS population by Pozzo et al. (2001). A similar explanation is likely for the Li-rich star RX 2 found in the NGC 2547 study of Jeffries et al. (2003). It lies 2 mag above the NGC 2547 PMS locus, exhibits undepleted Li and has an RV consistent with either NGC 2547 or Vela OB2. It is fortunate for membership studies in NGC 2547 that the distance/age combination of Vela OB2 places its low-mass population well above the NGC 2547 locus in CMDs.

6.3 Comparison of LDB ages with isochronal ages

The LDB ages determined for NGC 2547 and IC 2391 in Table 3 (and also the Alpha Per and Pleiades clusters – see Jeffries & Naylor 2001) are very precise thanks to the steep luminosity dependence of the age at which Li is burned in fully convective stars. These LDB ages are also likely to be very accurate in an absolute sense. The range of models we have employed use a wide variety of equations of state, radiative opacities, atmospheres and convective treatments and yet the difference between the largest and smallest age estimate in the case of NGC 2547 is only 1.9 Myr! Of course there is always a concern that some physics neglected by all the models may be important, such as rotation or the presence of supporting magnetic fields in the convection zone. Preliminary work suggests that the effects of these will be to increase the LDB ages, but only by a very small amount (Burke et al. 2004; F. D'Antona private communication). As the LDB ages are both precise and accurate they offer the opportunity to test the less well constrained physics that controls age determinations from higher mass stars.

6.3.1 Nuclear turn off ages

The LDB results for IC 2391, the Alpha Per and Pleiades clusters have shown that nuclear turn-off ages deduced from high mass stellar models without convective core overshooting are younger by factors of 1.5 than LDB ages (Barrado y Navascués et al. 2004). Unfortunately NGC 2547 may or may not be consistent with this picture. The nuclear turn-off age of NGC 2547 is ill-determined (55 ± 25 Myr based on models with a small amount of convective overshoot – Jeffries & Tolley 1998), mainly because it hinges on the photometry and reddening of just one star (HD 68478, not HD 68468 as stated in Jeffries & Tolley 1998).

6.3.2 Empirical low-mass isochrones in colour-magnitude diagrams

The ages of young clusters can also be derived rather precisely (but not necessarily accurately – see below) by fitting low-mass isochrones to cluster members in CMDs. The rate of descent towards the ZAMS is mass dependent but also depends somewhat on the treatment of convection and the details of the stellar atmospheres. Here NGC 2547 is an excellent cluster to check the consistencies of the age determinations. It has a well studied lower main sequence with very precise photometry and a well defined PMS locus. Unfortunately the absolute accuracy of the method is also dependent on how the model temperatures and luminosities are converted into colours and magnitudes before comparison with the data (or vice-versa).

In previous papers (e.g. Naylor et al. 2002; Oliveira et al. 2003; Jeffries et al. 2004) a method was described for empirically deriving the relationship between colour and $T_{\rm eff}$, using the well-observed Pleiades cluster as a calibrator. We assume the Pleiades distance and age are 132 pc and 120 Myr (roughly the LDB age) and adopt the same relationships between bolometric correction and colour as were used in deriving the LDB ages. Then, assuming the same colour-$T_{\rm eff}$ relation applies to clusters as young as NGC 2547 (which is not contradicted by theoretical atmosphere models), isochrones

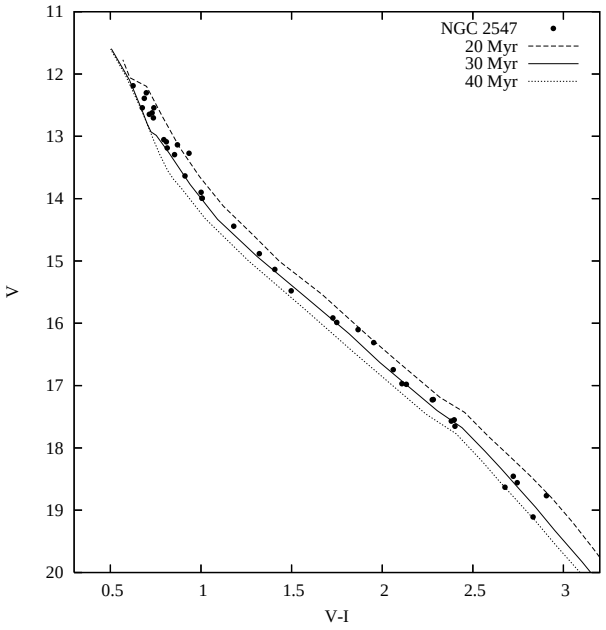

Figure 9. An example V versus $V-I$ CMD for presumed single, spectroscopically confirmed members of NGC 2547 (spots). Empirically calibrated isochrones at 20, 30 and 40 Myr are shown, derived from the theoretical models of Baraffe et al. (2002, with a mixing length parameter of 1.9 pressure scale heights) with a distance, reddening and extinction appropriate for NGC 2547.

Table 4. Empirical isochronal ages (in Myr) for NGC 2547

Evolutionary Model	CMD	
	V vs $V-I$	I vs $R-I$
D'Antona & Mazzitelli (1997)	24	26
Baraffe et al. (2002) (ML= 1.9 scale heights)	29	31
Baraffe et al. (2002) (ML= 1.0 scale heights	34	36
Siess et al. (2002) $z = 0.02$	26	28

can be generated to find a cluster age. The method is insensitive to the age assumed for the Pleiades and changing the Pleiades distance simply changes the distance to the fitted cluster by a similar factor (and hence the LDB age – see the discussion in Oliveira et al. 2003).

Figure 5 shows examples using the D'Antona & Mazzitelli (1997) and Baraffe et al. (2002, with a mixing length parameter of 1.9 pressure scale heights) models for an age of 30 Myr. Other examples of fits to NGC 2547 and IC 2391 covering stars at higher masses and in other CMDs can be found in Naylor et al. (2002), Oliveira et al. (2003) and Jeffries et al. (2004). We have uniformly reanalysed the V versus $V-I$ and I versus $R-I$ CMDs for NGC 2547 to estimate low-mass isochronal ages using the same models used to estimate the LDB ages. We have taken spectroscopically confirmed stars from Jeffries et al. (2000, 2003) and excluded those stars which were considered to be binary systems in an attempt to define a clean single star isochrone. For stars with $1.0 < V-I < 2.5$ and $0.5 < R-I < 1.5$, spectroscopically selected members of NGC 2547 lie on a very well defined PMS locus in the V versus $V-I$ and I versus $R-I$ CMDs (e.g. see Figs. 9 and 11). Warmer stars have already reached the ZAMS and offer no age discrimination. Cooler stars appear to show a more scattered PMS (see Figs. 5 and 11), due to a combination of variability and photometric errors, but may also suffer from systematic photometric calibration uncertainties.

Model isochrones were generated using the Pleiades as an empirical calibrator of the colour-$T_{\rm eff}$ relation and then matched to the NGC 2547 data using an intrinsic distance modulus of 8.1, (which is constrained by higher mass stars that have already reached the ZAMS) reddenings of $E(V-I) = 0.077$ and $E(R-I) = 0.043$ and the corresponding extinction values. The results are given in Table 4 and an illustrative example of the isochrone matching shown in Fig. 9. The ages deduced from the two CMDs are very consistent, but vary from about 25 Myr for the D'Antona & Mazzitelli (1997) models (a value independently arrived at by Stauffer et al. [2003] using a similar technique), up to about 35 Myr for Baraffe et al. (2002) models with a mixing length set to 1.0 pressure scale heights. The photometry available for the IC 2391 cluster is more scattered, but suggests an isochronal age that is 5 to 10 Myr older using any of these models.

The relative isochronal ages from different models are very precise because the alternative isochrones are almost parallel in the colour ranges considered. There are however uncertainties which shift the ages from all models approximately equally. The main sources of experimental error in this technique are the uncertainties in the adopted distance modulus and reddening of the cluster. Assuming the same values used to derive the LDB ages we find ∓ 5 Myr for a ± 0.1 mag change in distance modulus. This is a change in the same sense, but larger in magnitude than for the LDB age, where we find about ∓ 1.6 Myr for a ± 0.1 mag change in the distance modulus of NGC 2547. A ± 0.02 mag change in $E(B-V)$ results in a change in the derived intrinsic distance modulus (from the ZAMS stars) of about $\sim \pm 0.1$, but does not significantly change the isochronal age estimates from the lower mass stars since the reddening vector is close to parallel with the PMS isochrones in the CMDs. Statistical errors in deciding which isochrone fits best are only about ± 2 Myr for NGC 2547 where, for $1.0 < V-I < 2.5$ and $0.5 < R-I < 1.5$ the stars lie almost like "beads on a string". The scatter is greater at redder colours in NGC 2547 and also in IC 2391 at all colours, where an extra ± 5 Myr uncertainty in the isochronal age is warranted.

The main source of systematic error is the compatibility of the photometric calibrations of the Pleiades calibration data and the younger cluster data and the possibility that the colour-$T_{\rm eff}$ relation changes for stars with lower gravity. These factors are much less important for stars at 30 Myr with $R-I < 1.5$ and $V-I < 2.5$, which have gravities quite similar to Pleiades stars of the same colour and which are calibrated by many photometric standards of appropriate colour. We attach less weight to empirical isochrone comparisons for cooler stars, where gravities are lower than in the Pleiades, where the photometric calibration may be uncertain by ± 0.1 and where there appears to be more scatter in the photometry of genuine cluster members. However, even with these uncertainties it is encouraging that the empirical 30 Myr isochrones shown in Fig. 5 are certainly compatible with the data for the cooler stars observed in this paper.

Stauffer et al. (2003) have shown that the deduced isochronal age may also depend to a certain extent upon which colour indices are used. In particular they find that young, magnetically active stars suffer from a "blue excess" with respect to older stars. This would make ages determined from the V versus $B-V$ CMD problematic. However, they also show that this problem is much less serious using the V versus $V-I$ CMD upon which our empirical isochronal ages for NGC 2547 largely rest. In any case, by using the Pleiades as an empirical calibrator of the colour-$T_{\rm eff}$ relationship we potentially nullify these problems because the cool stars of NGC 2547 have very similar magnetic activity levels to those in the Pleiades (Jeffries & Tolley 1998). We also find that isochronal ages determined from the V versus $V-I$ and I versus $R-I$ CMDs are entirely consistent. The same may not be true when it comes to comparing theoretical isochrones with the NGC 2547 data, because the best theoretical atmospheres currently contain no contribution from chromospheres, spots or plages (see section 6.3.4).

The LDB age for IC 2391 is larger than its low-mass isochronal age when determined using the same models, although the discrepancy is perhaps not very significant at about 12 ± 8 Myr. It was partly this and partly the overestimate of the LDB age for NGC 2547 that led Oliveira et al. (2003) to speculate that LDB ages were *systematically higher* than isochronal ages in low-mass stars, perhaps indicating the need for new physics in the low-mass evolutionary models. Our new and precisely determined LDB age for NGC 2547 is only larger by a few Myr than the isochronal ages. The largest discrepancy occurs for the D'Antona & Mazzitelli (1997) models, and is only 10 ± 6 Myr. Discrepancies of this size could reasonably be accounted for by a small decrease in the cluster distance modulus of about its estimated error bar or could be due to small systematic changes in the colour-$T_{\rm eff}$ relationship with age.

6.3.3 The empirical temperature scale

The near consistency achieved between the LDB and isochronal ages is almost independent of the choice of model. This insensitivity to the chosen model arises from the intrin-

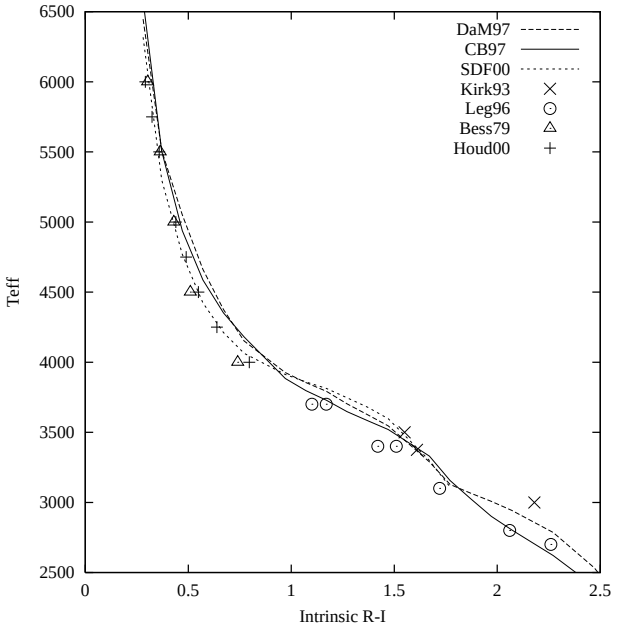

Figure 10. The relationship between intrinsic $R-I$ and $T_{\rm eff}$ derived by requiring evolutionary models to match Pleiades data at an age of 120 Myr and distance of 136 pc. The relationships for the Chabrier & Baraffe (1997 - CB97, with overshooting of 1.9 pressure scale heights), D'Antona & Mazzitelli (1997 - DaM97) and Siess et al. (2000 - SDF00, solar metallicity model) are shown. Also shown are the semi-empirical relationships found by Houdashelt et al. (2000 - Houd00) and Bessell (1979 - Bess79) and the empirical determinations of Kirkpatrick et al. (1993 - Kirk93) and Leggett (1996 - Leg96).

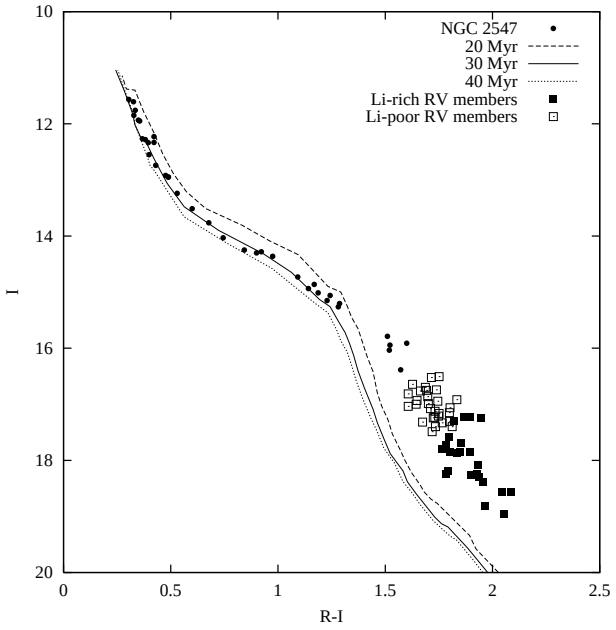

Figure 11. An I versus $R-I$ CMD for presumed single, spectroscopically confirmed members of NGC 2547 (spots) and the radial velocity members identified in this paper (squares). Isochrones at 20, 30 and 40 Myr are shown and taken directly from the theoretical models of Baraffe et al. (2002, with a mixing length parameter of 1.9 pressure scale heights) with a distance, reddening and extinction appropriate for NGC 2547.

sic similarity of the isochrones generated by the various models at this age, but also by our calibration technique of fixing the age of the Pleiades and hence deriving a slightly different relationship between colour and $T_{\rm eff}$ for each model. There *are* some differences in the isochrone shapes for cool young stars (see for instance Fig. 5), but unfortunately these occur at colours where uncertainties in the present photometric calibrations make it impossible to judge which models best describe the data.

In principle we could compare the required intrinsic colour-$T_{\rm eff}$ relationship with empirical and semi-empirical determinations of $T_{\rm eff}$ to see which model correctly describes this relationship. Figure 10 shows this comparison for $R-I$ versus $T_{\rm eff}$, the plot for $V-I$ versus $T_{\rm eff}$ is qualitatively very similar. Given the uncertainties in the empirical $T_{\rm eff}$ determinations – typically 200 K and the possible ±0.1 mag uncertainties in the photometric colours of very red stars we would be hard pressed to choose between the models in this way.

Finally, we can compare the $T_{\rm eff}$ at which the models predict the LDB (listed in Table 3) with the $T_{\rm eff}$ corresponding to the colour of the LDB from Fig. 10. The $T_{\rm eff}$ at the LDB ranges from 3250 K, for the Chabrier & Baraffe (1997) models (which use a detailed model atmosphere) to 3140 K for the D'Antona & Mazzitelli (1997) models (which use a grey atmosphere). The derived *intrinsic* $(R-I)$-$T_{\rm eff}$ relations in Fig. 10 give very similar $T_{\rm eff}$ values for all the models of 3185-3220 K at $(R-I)_0 = 1.73$. Given the possible 0.1 mag uncertainties in $R-I$, corresponding to $T_{\rm eff}$ uncertainties of ~ 150 K, all the models are satisfactory in the sense that the isochronal $T_{\rm eff}$ at the colour of the LDB and the theoretical $T_{\rm eff}$ at the LDB are consistent.

6.3.4 Comparison with theoretical low-mass isochrones

A purer test of the consistency between the LDB and low-mass isochronal ages is available using the models of Baraffe et al. (2002). These models, based on the evolutionary code of Chabrier & Baraffe (1997), predict both Li-depletion *and* the photospheric colours and magnitudes using complex model atmospheres.

Figure 7 includes theoretical isochrones adjusted for an intrinsic distance modulus of 8.1 mag and reddening of $E(I-K_s) = 0.092$. These suggest an age of 25 ± 5 Myr for NGC 2547, but there are additional errors due to the systematic photometric uncertainty of ±0.1 in the I magnitudes of these cool stars, ±0.031 in $E(I-K_s)$ and ±0.1 in the distance modulus. Hence the age from this method is 25 ± 7 Myr, again in reasonable agreement with the LDB age found from the same stars and evolutionary models. The K_s versus $I-K_s$ diagram for stars in IC 2391 around its LDB suggests an age of 40 ± 10 Myr, also in reasonable agreement with the LDB age (see Fig. 9b of Barrado y Navascués et al. 2004).

The cool stars we have considered here have rather imprecise 2MASS near IR magnitudes. To improve on this we use the spectroscopically confirmed sample of brighter NGC 2547 stars discussed in section 6.3.2. The comparisons between theory and data are shown in Figs. 11, 12 and 13. Note that the Baraffe et al. (2002) colours and magnitudes on the

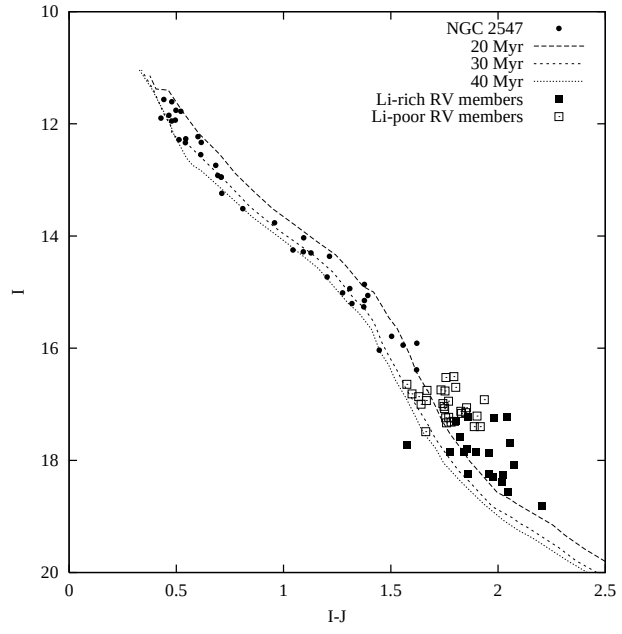

Figure 12. An I versus $I-J$ (2MASS system) CMD for NGC 2547. Symbols and lines are as for Fig. 11

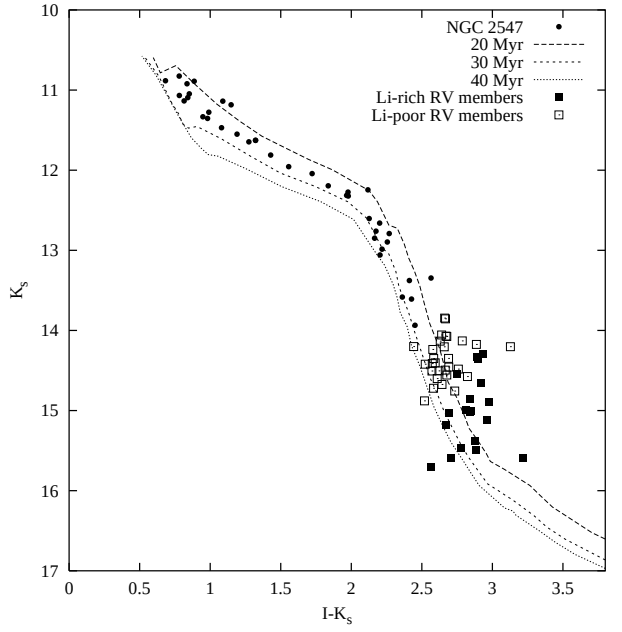

Figure 13. A K_s versus $I-K_s$ (2MASS system) CMD for NGC 2547. Symbols and lines are as for Fig. 11

CIT system have been converted to the 2MASS system for these plots.

The agreement between the LDB age of NGC 2547 from the Chabrier & Baraffe (1997) models (35 ± 3 Myr) and the theoretical isochrone fits from the same models is also very good. The theoretical I versus $R-I$ isochrones, like the empirical isochrone modelling in Jeffries et al. (2004), suggest an age of 30 ± 5 Myr for $R-I < 1.2$, the I versus $I-J$ plot suggests an age of (30 ± 5) Myr for $I-J < 1.5$, whilst the I versus $I-K_s$ CMD suggests an age of (25 ± 5) for $I-J < 3$. In all the CMDs, but particularly for I versus $R-I$ there is a hint that the stars are not arrayed parallel to the isochrones even in these colour ranges. At redder colours this becomes more than a hint. The data and models are clearly discrepant at any age for $R-I > 1.2$ (a deficiency in the models already noted by Baraffe et al. [1998] and probably due to missing atmospheric molecular opacity in the optical spectrum of cool objects) and a drift of stars towards younger ages for $I-J > 1.5$ is also apparent. However, recall that systematic errors of order 0.1 mag are possible in the colours of the red stars so overall the theoretical NIR colours and models do a reasonably good job of modelling the NGC 2547 data at or just below the LDB age derived from the same model. It is interesting to note though that the theoretical model atmospheres do not simulate spots, plages, chromospheres or other manifestations of magnetic activity in these young stars. Stauffer et al. (2003) found that cool Pleiades stars seemed to show a small K-band excess with respect to older stars. There is a hint of this also in our data, where the K versus $I-K$ CMD gives a lower isochronal age than the other CMDs. This would be brought back into line by the addition of a $\simeq 0.1$ mag $I-K$ excess in the model atmospheres.

7 CONCLUDING REMARKS

Deep, intermediate resolution spectroscopy obtained with the VLT/GIRAFFE spectrograph has been used to study a group of 63 low-mass ($0.08-0.3\,M_{\odot}$) candidate members of the young open cluster, NGC 2547. Radial velocity measurements and the presence of strong Li I 6708Å absorption in the fainter stars, have confirmed membership for at least 50 objects. We have hence validated previous work that selected low-mass members and estimated the extent of sample contamination based solely on photometric selection (Jeffries et al. 2004). The conclusions of that work regarding the mass function and luminosity function of NGC 2547 should be sound, at least down to the substellar boundary.

From the sample of confirmed members we have determined the magnitude at which lithium switches from being completely depleted, to being found close to its initial abundance, as $I = 17.54 \pm 0.14$, $K_s = 14.86 \pm 0.12$ and at colours of $R-I = 1.77 \pm 0.03$ and $I-K_s = 2.70 \pm 0.12$.

Using several PMS evolutionary models which incorporate a variety of physical approximations we find an almost model-independent lithium depletion boundary age (LDB) of 34-36 Myr, with a precision of 10 per cent. This LDB age is only slightly larger than the ages of 25-35 (± 5) Myr deduced from isochrone fits to stars from 0.08-1.2$M_{\odot}$ using the same models and empirically calibrated relationships between colour, bolometric correction and $T_{\rm eff}$. It is also slightly larger than ages of 25-30 (± 5) Myr deduced from isochrone fits in the $I, I-J$ and $I, I-K_s$ CMDs using only the theoretical colours and magnitudes of Baraffe et al. (2002). However, perfect agreement with the LDB ages can be obtained with a distance reduction to the cluster of only 0.1 mag, approximately equal to its estimated error bar.

On the basis that the isochrone fits to low-mass are compatible with LDB ages derived from the same models we find that all of the PMS models we have considered (Chabrier & Baraffe 1997; D'Antona & Mazzitelli 1997; Siess et al.

2000, Baraffe et al. 2002) give acceptable results. This is despite possible systematic uncertainties regarding the intrinsic colours of cool, magnetically active young stars (Stauffer et al. 2003). At the age of NGC 2547, significant differences in the isochrones predicted by these models occur at colours so red that uncertainties in photometric calibration prevent any decisive test between them. However, this result now seems to remove any pressing need to introduce new physics such as rotation or extra magnetic support into the PMS models and lends confidence to isochronal ages determined (using the methods outlined here) from low-mass stars between 30 and 120 Myr. This is an important result, because PMS isochronal ages can easily be determined from photometry obtained on small telescopes, whereas even for nearby clusters, determining LDB ages stretches the capabilities of 8-m telescopes.

The differences in the isochrones predicted by the various flavours of model, arising from variations in their treatment of convection, atmospheres, equations of state and interior opacities, become more apparent at younger ages. This work demonstrates that finding the LDB is certainly possible down to $I \simeq 18.5$ and therefore the technique could and should be applied to more distant clusters in the 10-20 Myr age range.

ACKNOWLEDGMENTS

We would like to thank the staff of the VLT in Paranal for delivering a superb dataset in service mode. Data reduction was performed on computing facilities at Keele University funded by the UK Particle Physics and Astronomy Research Council (PPARC). JMO acknowledges financial support from PPARC. We thank Tim Naylor for useful discussions. This publication makes use of data products from the Two Micron All Sky Survey, which is a joint project of the University of Massachusetts and the Infrared Processing and Analysis Center/California Institute of Technology, funded by the National Aeronautics and Space Administration and the National Science Foundation.

REFERENCES

Baraffe I., Chabrier G., Allard F., Hauschildt P. H., 1998, A&A, 337, 403
Baraffe I., Chabrier G., Allard F., Hauschildt P. H., 2002, A&A, 382, 563
Barrado y Navascués D., Stauffer J. R., Jayawardhana R., 2004, ApJ, in press
Barrado y Navascués D., Stauffer J. R., Patten B. M., 1999, ApJ, 522, L53
Bessell M., 1979, PASP, 91, 589
Bildsten L., Brown E. F., Matzner C. D., Ushomirsky G., 1997, ApJ, 482, 442
Blecha A., North P., Royer F., Simond G., 2003, Technical report, GIRAFFE BLDR Software Reference Manual Version 1.09. Observatoire de Genève
Burke C. J., Pinsonneault M. H., Sills A., 2004, ApJ, 604, 272
Carpenter J. M., 2001, AJ, 121, 2851
Chabrier G., Baraffe I., 1997, A&A, 327, 1039
Chiosi C., Bertelli G., Bressan A., 1992, ARA&A, 30, 235
Clariá J. J., 1982, A&AS, 47, 323
Cutri, R. M. et al. 2003, Technical report, Explanatory supplement to the 2MASS All Sky data release. http://www.ipac.caltech.edu/2mass/
D'Antona F., Mazzitelli I., 1997, Mem. Soc. Astr. It., 68, 807
de Zeeuw P. T., Hoogerwerf R., de Bruijne J. H. J., Brown A. G. A., Blaauw A., 1999, AJ, 117, 354
Gizis J. E., Reid I. N., Hawley S. L., 2002, AJ, 123, 3356
Houdashelt M. L., Bell R. A., Sweigart A. V., 2000, AJ, 119, 1448
Houdebine E. R., Doyle J. G., 1995, A&A, 302, 861
Jeffries R. D., Naylor T., 2001, in Montmerle T., André P., eds, From darkness to light: Origin and evolution of young stellar clusters ASP Conference Series, Vol. 243, San Francisco, p. 633
Jeffries R. D., Naylor T., Devey C. R., Totten E. J., 2004, MNRAS, 351, 1401
Jeffries R. D., Oliveira J. M., Barrado y Navascués D., Stauffer J. R., 2003, MNRAS, 343, 1271
Jeffries R. D., Tolley A. J., 1998, MNRAS, 300, 331
Jeffries R. D., Totten E. J., James D. J., 2000, MNRAS, 316, 950
Kenyon M. K., Jeffries R. D., Naylor T., Oliveira J. M., Maxted P. F. L., 2004, MNRAS, in press
Kirkpatrick D., Kelly D., Rieke G., Liebert J., Allard F., Wehrse R., 1993, ApJ, 402, 643
Leggett S. K., Allard F., Berriman G., Dahn C. C., Hauschildt P. H., 1996, ApJS, 104, 117
Meynet G., Maeder A., 1997, A&A, 321, 465
Meynet G., Maeder A., 2000, A&A, 361, 101
Meynet G., Mermilliod J. C., Maeder A., 1993, A&AS, 98, 477
Naylor T., Totten E. J., Jeffries R. D., Pozzo M., Devey C. R., Thompson S. A., 2002, MNRAS, 335, 291
Oliveira J. M., Jeffries R. D., Devey C. R., Barrado y Navascués D., Naylor T., Stauffer J. R., Totten E. J., 2003, MNRAS, 342, 651
Pinsonneault M. H., Stauffer J. R., Soderblom D. R., King J. R., Hanson R. B., 1998, ApJ, 504, 170
Pozzo M., Jeffries R. D., Naylor T., Totten E. J., Harmer S., Kenyon M., 2000, MNRAS, 313, L23
Pozzo M., Jeffries R. D., Naylor T., Totten E. J., Harmer S., Kenyon M., Walter F. M., 2001, in Montmerle T., André P., eds, From darkness to light: Origin and evolution of young stellar clusters ASP Conference Series, Vol. 243, San Francisco, p. 801
Rieke G. H., Lebofsky M. J., 1985, ApJ, 288, 618
Siess L., Dufour E., Forestini M., 2000, A&A, 358, 593
Stauffer J. R., Barrado y Navascués D., Bouvier J., Morrison H. L., Harding P., Luhman K., Stanke T., McCaughrean M., Terndrup D. M., Allen L., Assouad P., 1999, ApJ, 527, 219
Stauffer J. R., Hartmann L. W., Barrado y Navascués D., 1995, ApJ, 454, 910
Stauffer J. R., Jones B. F., Backman D., Hartmann L. W., Barrado y Navascués D., Pinsonneault M. H., Terndrup D. M., Muench A. A., 2003, AJ, 126, 833
Stauffer J. R., Schultz G., Kirkpatrick J. D., 1998, ApJ, 499, L199
Ushomirsky G., Matzner C. D., Brown E. F., Bildsten L., Hilliard V. G., Schroeder P. C., 1998, ApJ, 497, 253
White R. J., Basri G., 2003, ApJ, 582, 1109
Young E. T. amd Lada C. J., Teixeira P., Muzerolle J., Muench A., Stauffer J., Beichman C. A., Rieke G. H., Hines D. C., Su K. Y. L., Engelbracht C. W., Gordon K. D., Misselt K., Morrison J., Stansberry J., Kelly D., 2004, ApJS, 154, 428
Zapatero Osorio M. R., Béjar V. J. S., Pavlenko Y., Rebolo R., Allende Prieto C., Martín E. L., García López R. J., 2002, A&A, 384, 937

This paper has been typeset from a TEX/ LATEX file prepared by the author.